Lubricated Pipelining: Stability of Core-Annular Flow V: Experiments and comparison with theory

by

Runyuan Bai, Kangping Chen and D. D. Joseph

Department of Aerospace Engineering and Mechanics
University of Minnesota
107 Akerman Hall
110 Union Street SE
Minneapolis, MN 55455

April, 1990

Contents

Abstract

Results are given for experiments on water lubricated pipelining of 6.01 poise cylinder oil in a vertical apparatus in up and down flow in regimes of modest flow rates, less than 3 ft/sec. Measured values of the flow rates, holdup ratios, pressure gradients and flow types are presented and compared with theoretical predictions based on ideal laminar flow and on the predictions of the linear theory of stability. New flow types, not achieved in horizontal flows, are observed: bamboo waves in up flow and corkscrew waves in down flow. Nearly perfect core annular flows are observed in down flows and these are nearly optimally efficient with values close to the ideal. The holdup ratio in up flow and fast down flow is a constant independent of the value and the ratio of values of the flow rate of oil and water. A vanishing holdup ratio can be achieved by fluidizing a long lubricated column of oil in the down flow of water. The results of experiments are compared with computations from ideal theory from perfect core annular flow and from the linear theory of stability. Satisfactory agreements are achieved for the celerity and diagnosis of flow type. The wave is shown to be nearly stationary, convected with the oil core in this oil and all oils of relatively high viscosity. These results are robust with respect to moderate changes in the values of viscosity and surface tension. The computed wave lengths are somewhat smaller than the average length of bamboo waves which are observed. This is explained by stretching effects of buoyancy and lubrication forces induced by the wave. Other points of agreement and disagreement are reviewed.

Nomenclature

a	$= R_2/R_1$ radius ratio
A	$= \pi R_2^2$ where $R_2\left(\frac{3}{16}\text{ in}\right)$ is the inside radius of the pipe
BW	= Bamboo waves (see figures 5.3, 9.1–9.9)
CW	= Corkscrew wave (see figures 4.1, 9.4)
d	$= 2R_2$
DBW	= Disturbed bamboo waves (see figure 5.6)
DCAF	= Disturbed core annular flow (see figures 5.7, 9.9)
η	$= R_1/R_2 = 1/a$ radius ratio
$f_1 f_2$	= pressure gradients (8.8)
H_1	$= H_o$ height of oil head
H_2	$= H_w$ height of water head
$\hat{H}, \hat{H}_1, \hat{H}_2$	= heights of water columns in the manometer tube (see figure 3.2)
h	= holdup ratio (4.1)
J	$= \pi R_2/a\rho_1 v_1^2$ capillary number of Chandrasekhar
J^*	$= aJ$
L	$= H_o + H_w$
m	$= \mu_2/\mu_1$ viscosity ratio (oil inside corresponds to m<1). In the experiments M=1/601 at 22°C)
μ_1	$= \mu_o$ oil viscosity
μ_2	$= \mu_w$ water viscosity
ν	= kinematic viscosity; μ/ρ; $\nu_1=\nu_w$, $\nu_2=\nu_o$.
Ω_o	$= H_o\pi R_1^2$ volume of oil
Ω_w	$= H_w\pi(R_2^2 - R_1^2)$ volume of water
Ω	$= \Omega_o + \Omega_w$ total volume
$\hat{P}$	= piezometric pressure
p	= dynamic pressure
p'	= constant pressure gradient
PCAF	= perfect core annular flow
Q_1	$= Q_o$ volume flow rate of oil
Q_2	$= Q_w$ volume flow rate of water
R_1	= mean radius of the oil/water interface
R_2	= inside radius of the pipe
$\leftarrow$	$= W_o d/\nu$ Reynolds number (see W_o)
$\leftarrow e$	$= Vd/\nu$ Reynolds number (see V)
$\leftarrow g(R_1)$	$= R_1\sqrt{rR_1}\ /\ \nu_1$ Reynolds number
ρ_1	$= \rho_o$ oil density
ρ_2	$= \rho_w$ water density
T	= interfacial tension
(V, V_1, V_2)	$= (V, V_o, V_w) = (Q, Q_o, Q_w)/A$ are superficial velocities
$W(r)$	= axial velocity of PCAF

W_o = W(0) centerline velocity
W(1) = velocity of oil/water interface in PCAF

1. Introduction

The motivation for the work done in this paper and the results so far achieved are explained in the papers on the title topic which precede this one: Joseph, Renardy and Renardy [JRR, 1985]; Preziosi, Chen and Joseph [PCJ, 1989]; Hu and Joseph [HJa, 1989]; Hu and Joseph [HJb, 1989]; Chen, Bai and Joseph [CBJ, 1989]; Chen and Joseph [CJ, 1990]; and Hu, Lundgren and Joseph [HLJ, 1990].

This paper reports the results of experiments on core-annular flow in a vertical pipe and correlates the observations with the results of computations using ideal theory and the linear theory of stability. The ⊓ tube apparatus used in these experiments was described by CBJ but we will describe it in more detail in §3. The force of gravity is axial in this apparatus, in the direction of the pressure gradient in up flow and against the pressure gradient in down flow. We can account for all the principal physical effects in the stability study of these flows; the effects of the viscosity difference, the density difference, gravity, surface tension and the Reynolds number.

The flow charts presented in this paper are the first for vertical flow and surprising results for the holdup ratio and the pressure gradient reduction are reported. The comparison of linear theory and experiments is the most extensive one so far reported and we find agreement between theory and experiments in certain specific regimes of flow.

2. Fluid properties

The experiments reported here have been going on for over two years. The Mobil cylinder oil we use is recycled again in a closed system in which oil and water are put into repeated contact. After two years the recycled oil has taken on water in a relatively stable emulsion. We have samples of the fresh oil and the emulsion of water droplets in oil. The viscosity of the emulsified oil is less than half that of the pure oil. It is well known that emulsification of water into oil will increase the viscosity, as in Einstein's formula. Tipman and Hodgson [1956] measured the viscosity for solutions of water emulsified in oil in concentrations ranging up to 30%. Except for an observed small decrease in viscosity at a water fraction of 2.5%, the emulsions of water in oil had increasingly larger viscosities. Both oils are Newtonian, without shear thinning, as shown in figure 2.1. Viscosity vs. temperature graphs are shown in figure 2.2. We don't have an explanation of the decrease in viscosity of the water emulsified oil, the decrease is greater even than for an ideal mixture computed as follows. If ε is the water fraction, the density ρ_e of the emulsion is the weighted sum $\varepsilon\rho_w+(1-\varepsilon)\rho_o$ of density of water/oil and $\mu_e=\varepsilon\mu_w+(1-\varepsilon)\mu_o$. The density $\rho_e=0.905$ g/cm^3 and $\rho_o=0.885$ g/cm^3. Hence $\varepsilon=2/11.5$. At 22°, $\mu_o=13.8$p and $\mu_e\sim 9.5(13.8)/11.5=11.4$ poise. This is much larger than the measured value $\mu_e=6.01$ poise. It is possible that the emulsified oil contains air. Another possibility is that the oil has undergone chemical change in two years, possibly due to attack by bacteria.

The viscosity of the pure oil and the used oil was measured on a Rheometrics System 4 rheometer and on a parallel plate Deer rheometer with consistent results. The water used in our experiments was a 0.4% aqueous solution of sodium silicate. The density of this solution is $\rho_w=0.995$ gm/cm^3 and the viscosity is taken at $\mu_w=10^{-2}$ poise. The sodium silicate was added to promote wettability of the glass walls of the pipe with water, to promote lubrication. This works if the glass is clean. After two years without cleaning, the dirty walls are less hydrophilic to aqueous sodium silicate solution than clean walls to pure water. The nature of absorbed layers, and the history of wetting are

important; wetting is not just a property of materials but depends on the history and dynamics of fluid motions near a surface (see (vi) of §5 for more discussion).

The interfacial tension was measured with a spinning rod tensiometer (Than, et al [1988]) which is basically a spinning drop tensiometer with a centrally located rod of small diameter designed to improve spin up and stability. Measurement were taken with and without a rod, with good agreements. The interfacial tension between emulsified oil and pure water is T=22.50±1.86 dyn/cm. The interfacial tension between emulsified oil and the aqueous sodium silicate solution is T=8.54±0.157.

For our computations we have used measured values for the emulsified oil and sodium silicate solution at T=22°.

$$(\mu_w, \mu_o) = (10^{-2}, 6.01) \text{ poise},$$
$$(\rho_w, \rho_o) = (0.995, 0.905) \text{ gm/cm}^3,$$
$$T = 8.54 \text{ dyn/cm}. \tag{2.1}$$

At an earlier time we computed values for pure oil which we believed were right for the experiment, but they do not characterize the fluids for which data was taken correctly. We are going to present some computations in §10 for this oil.

$$(\mu_w, \mu_o) = (10^{-2}, 13.32) \text{ poise},$$
$$(\rho_w, \rho_o) = (1, 0.881) \text{ gm/cm}^3,$$
$$T = 20 \text{ dyn/cm}. \tag{2.2}$$

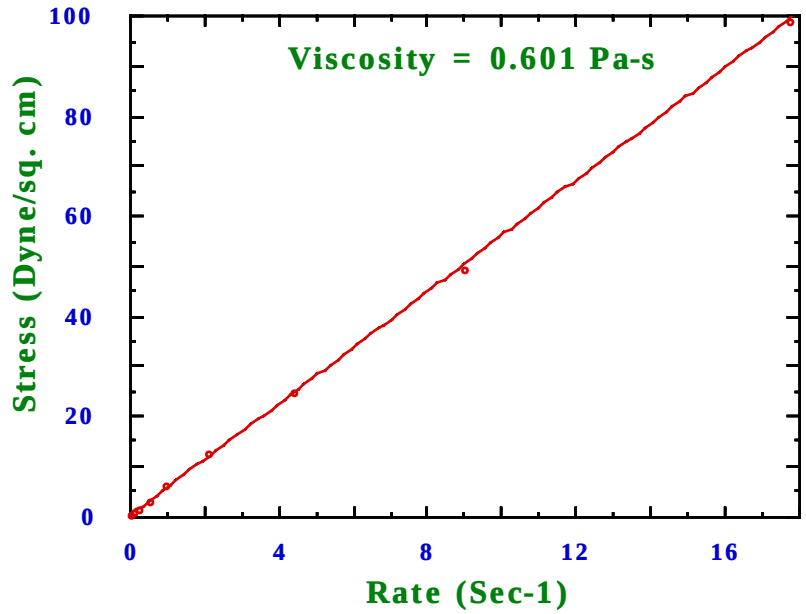

(a)

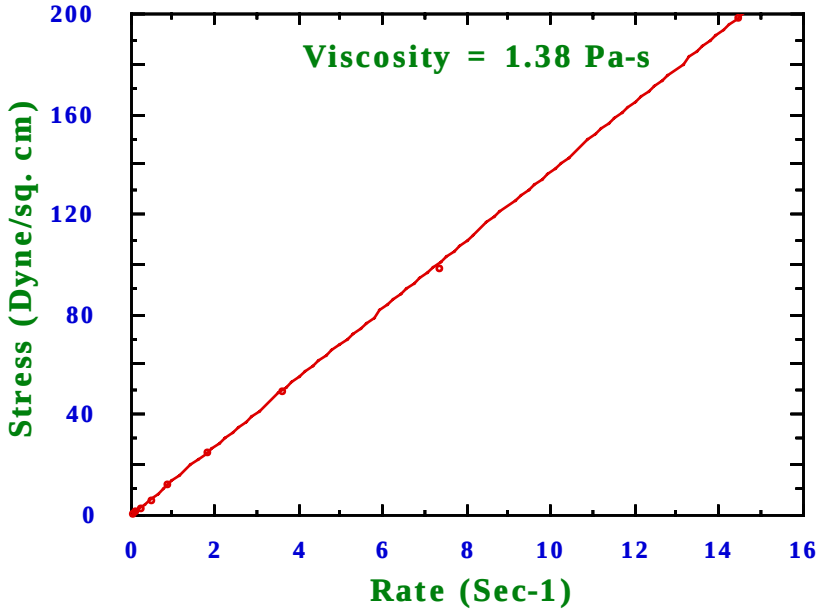

(b)

Figure 2.1 The shear stress is a linear function of the shear rate in the emulsified (a) and unemulsified (b) oil at T = 22 °C.

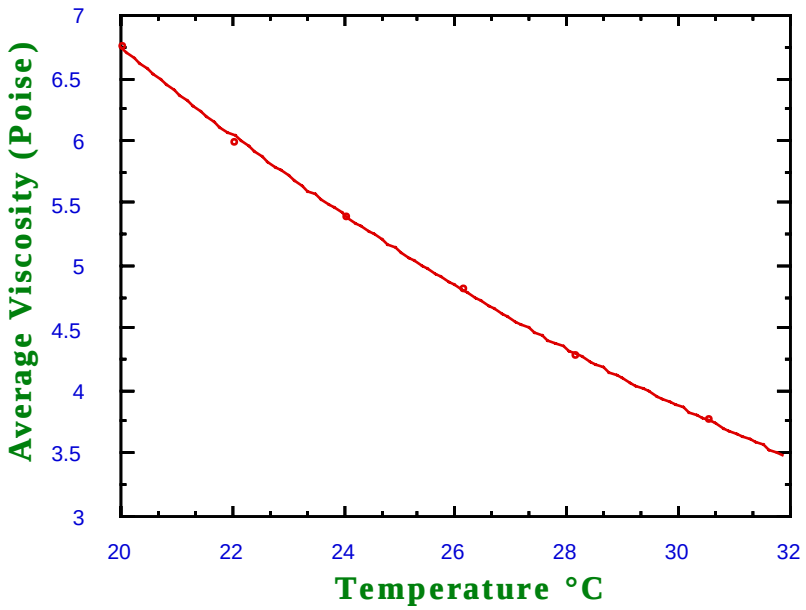

Figure 2.2 Viscosity of used water in oil emulsion as a function of temperature.

3. Experimental setup and procedures

The flow system is shown in figure 3.1. The pipeline is a ∩ loop which is mounted on the wall with its long legs vertical, aligned with gravity. The flow of oil and water to the pipeline is established by the pressure of compressed air in the oil and water tanks. The flow rates Q_o and Q_w or oil and water are controlled by valves at the outlet of the oil and water tanks. Q_w is measured by a Dwyer rotameter and Q_o by a positive displacement gearmeter (FTB-1000, manufactured by Omega Engineering Co.) which is particularly suited for high viscosity liquids. The oil and water are injected into the pipeline concentrically in an oil core and water annulus flow by means of a nozzle fitted centrally in the pipe. Water flows in the pipe and oil in the nozzle. We have nozzles of different diameters. The "best" diameter depends on flow conditions. The flow is first pushed up against gravity in the left leg of the ∩ loop. The flow turns around at the top of the loop and flows down in the right leg. There are test sections on the left and right legs which are enclosed in boxes filled with glycerine to remove lens distortion from the round walls of the pipe. The height of test sections is 93". The total height of the ∩ loop is 180".

The ∩ loop system is closed, the oil and water are recirculated. Oil and water are stored in separate pressurized tanks. The pressure levels in the two tanks are adjustable and drive the liquids to the ∩ loop without pulse. The oil and water are ejected into a large tank and separated under gravity. After separation the two liquids are driven back into the inlet storage oil tanks by compressed air.

Pressure drops are measured in the up and down flow legs of ∩ loop. In each leg there are two pressure taps connected to a manometer. The pressure taps are designed to facilitate the separation of oil from the water so that only water will enter the manometer. The pressure gradient cannot simply read off the manometer when there are two fluids in the pipe. Let $\hat{P}_A$ be the piezometric pressure at the bottom tap in figure 3.2 and $\hat{P}_B$ is the piezometric pressure at the top tap. The pressure difference

$$\hat{P}_A - \hat{P}_B = \rho_w g H_w + \rho_o g H_o + \Delta p \tag{3.1}$$

where $\rho_w g H_w$ is the weight of the water, $\rho_o g H_o$ the weight of the oil per unit area and

$$\Delta p = p_A - p_B \tag{3.2}$$

is the dynamic pressure producing flow. Now consider the manometer in figure 3.2(a) and let $\hat{P}_C$ be the air pressure in the column of air separating the two legs of the manometer. The pressure at A balances P_C plus the pressure of the water column of height $\hat{H}_1$,

$$\hat{P}_A = \hat{P}_C + \rho_w g \hat{H}_1 . \tag{3.3}$$

The pressure $\hat{P}_C$ balances $\hat{P}_B$ plus the pressure of column of water of $L - \hat{H}_2$ where L is the distance A to B

$$\hat{P}_C = \hat{P}_B + \rho_w g (L - \hat{H}_2) . \tag{3.4}$$

Combining now (3.1), (3.3), (3.4) and

$$L = H_o + H_W \tag{3.5}$$

we find that

$$\Delta p = \rho_w g \hat{H} + (\rho_w - \rho_o) g H_o \tag{3.6}$$

is the pressure drop due to motion up flow.

In down flow where the pressure gradient and relative buoyancy are opposed, the height difference of the manometer legs is proportional to Δp *plus* the hydrostatic contribution so that

$$\Delta p = \rho_w g \hat{H} - (\rho_w - \rho_o) g H_o \tag{3.7}$$

We may have flow, due to relative buoyancy alone for which $\hat{H} = 0$.

Formulas (3.6) and (3.7) require measured values of H and H_o. The height difference H is read directly but H_o depends on the volume of oil between the pressure taps in the pipe and it cannot be determined directly.

To determine H_o, we measure the volumes of oil and water between the pressure taps directly. This is done by means of two valves, called holdup valves, which cut off the flow between the taps simultaneously. There is a third safety valve which opens at the same time that the holdup valves are closed, releasing the high pressure in the system. After the holdup valves are closed, the oil rises and the volumes of oil and water are read easily. Actually the distance between the holdup valves is 93 inches so that the measured heights must be reduced by 90/93. Since the diameter (d=3/8 inches) of all pipes is the same, we may easily compute volumes by measuring heights. There are two sets of holdup valves, one for up flow and one for down flow.

All the data taken in our experiments is recorded on our Kodak Spin Physics high speed video camera or on a high resolution video camera. The only quantities that can be controlled after an experiment is in place are the flow rates of oil and water. We fix one of the flow rates and vary the other. Then we wait for transients to decay. The slower flow rates have long transients. After steady conditions are established, video recordings are made. The high speed recordings have the raw data for the analyses of flow. We can see the flow in slow motion; we can stop the flow or step advance the flow on the high speed video recording. This allows us to measure the distances, say between crests of waves and their phase speed (celerity). The size and speed of slugs and bubbles and the correlation of flow types with operating conditions can all be determined from these video recordings. For this paper we have been interested in flow type and average wave lengths and wave speeds. These are simple averages obtained by summing values and dividing by the number of trials. Our stored data can also be analyzed for the spectral properties of the waves, which should be useful for projected studies of the nonlinear properties of wavy flow.

To correlate the experimental observations with the linear theory of stability, we need to specify whether we are in up or down flow, the two flow rates and the water fraction in the pipe. The water fraction is a functional of the solution determined by the holdup ratio in the manner described below.

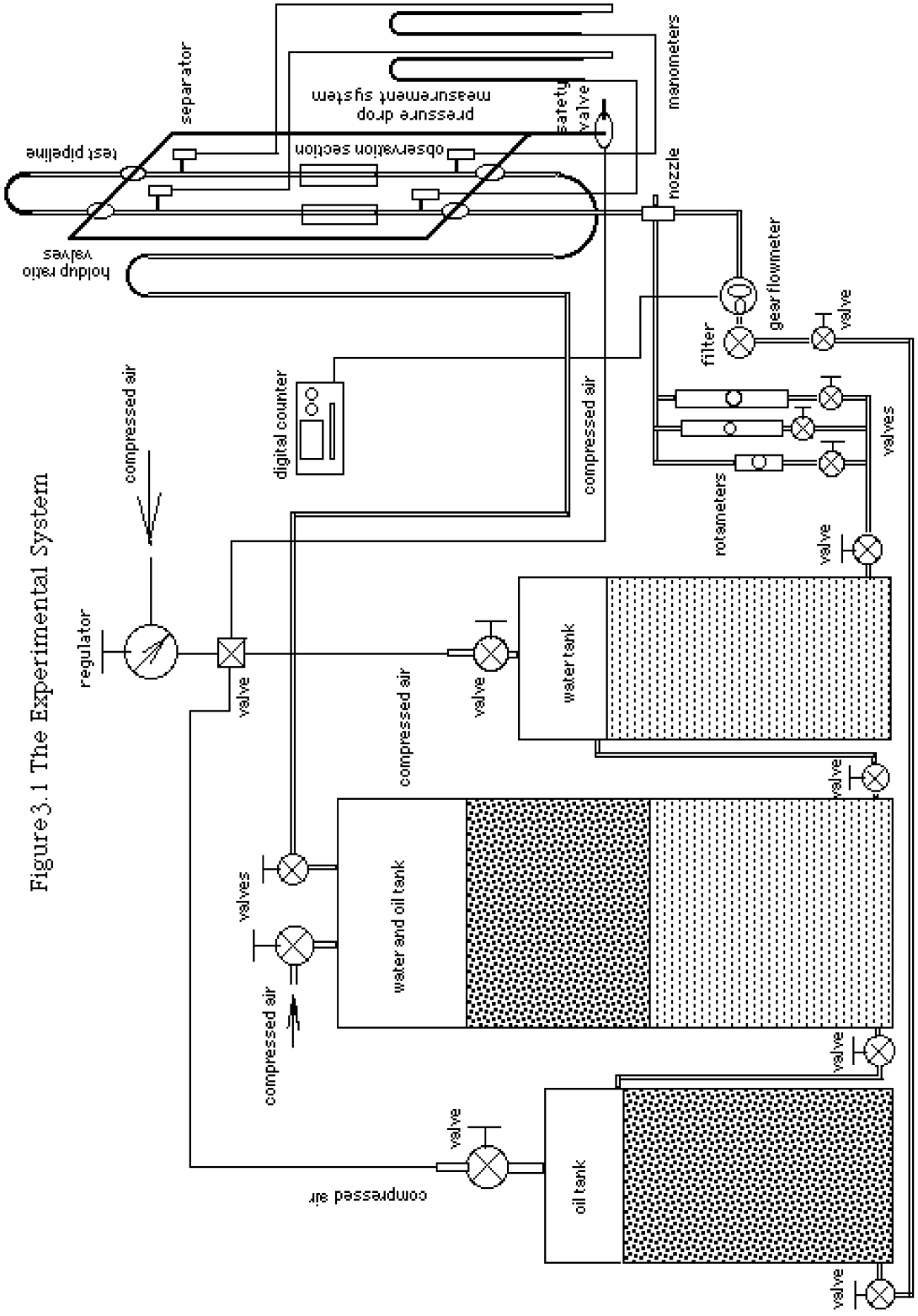

Figure 3.1 The experimental system.

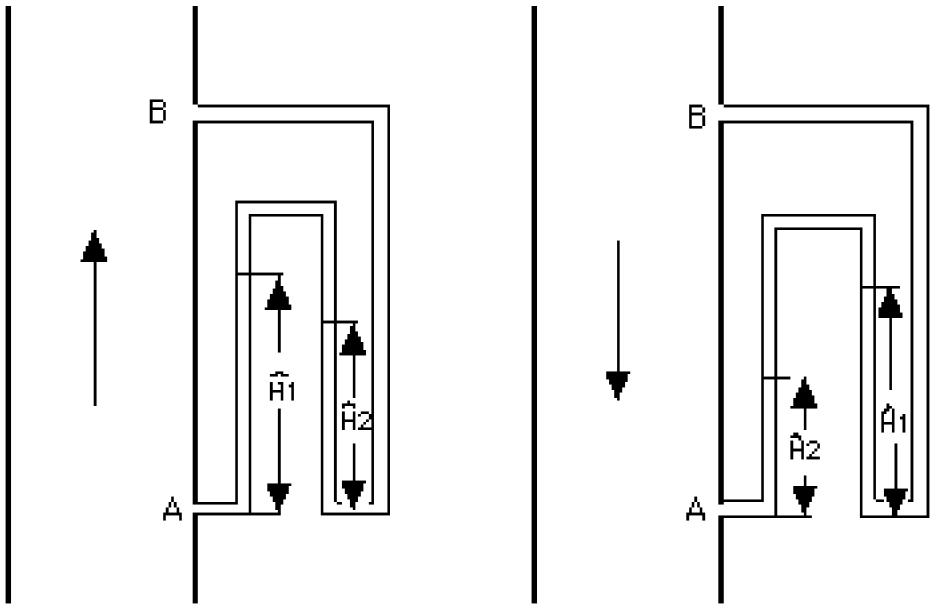

Figure 3.2 Manometer tubes in up flow (a) and down flow (b). The distance from A to B is L and $\hat{H}_1 - \hat{H}_2 = \hat{H}$. In flows driven by buoyancy alone, without pressure gradients, $\hat{H} < 0$.

4. Holdup ratio in up flow and down flow

Conventional wisdom about holdup ratios in lubricated pipelining needs to be amended for effects of buoyancy in vertical pipes. The holdup ratio is the ratio of ratios, the ratio (4.1) of volume flow rates to the ratio of volumes. These two ratios would be the same in a perfectly mixed flow, say a well-emulsified solution of water in oil. In the perfectly mixed flow the holdup ratio h is one. In general, and certainly in lubricated pipelining, the two fluids are not well-mixed and the holdup ratio differs from unity. The conventional wisdom is that the liquid in contact with the pipe wall tends to be held back. Thus the holdup will tend to be greater than unity when the water is the component in contact with the pipe wall and to be less than unity when oil is in contact with the pipe wall. This idea is not correct in vertical flow where the effects of buoyancy are important.

Because the up and down flow legs of our ∩ loop apparatus are connected, the pressure drop is established over the whole pipe with a continuous loss of pressure due to friction. The reader may be helped by thinking that to a first approximation the pressure gradient is a constant, the same constant in the up and down legs of the ∩ apparatus. Gravity aids the applied pressure gradient in accelerating the oil relative to water in the up flow and decelerating the oil relative to the water in the down flow legs of the apparatus. This means that more oil accumulates in down flow than in up flow. The water fraction is greater in up flow than in down flow. This implies that the $a-1=(R_2-R_1)/R_1$ is smaller in down flow and that the holdup ratio

$$h = (Q_o/Q_w) / (\Omega_o/\Omega_w) = (V_o/V_w) / (H_o/H_w) \tag{4.1}$$

is smaller in down flow where $\Omega_o=\pi R_2^2 H_o$, the oil volume, is larger.

The value h=0 of the holdup ratio can never be achieved in up flow or horizontal flow, but it can be realized in down flow. We get h=0 when there is already oil in the pipe, $\Omega_o\neq 0$, but no new oil supply is forthcoming, $Q_o=0$. An experimental realization of this in down flow is shown in Figure 4.1 where a long slug oil with aspect ratio in excess of 20 is exhibited. This slug is perfectly lubricated by water.

Basically we can say that the slug is fluidized, it is lifted by gravity against the oncoming down flow of water, suspended in the lubricating stream in an equilibrium of weight and drag. It is possible to suspend truly large slugs with aspect ratios greater than 100 in this way.

The volume ratio $\Omega_o/\Omega_w=H_o/H_w$ is per unit length of pipe, hence equal to the area ratio A_o/A_w of oil to water in a perfect core annular flow. This ratio may be expressed in terms of the radius ratio $a=R_2/R_1$ by the formula $a^2-1=A_w/A_o$. After replacing Ω_w/Ω_w with a^2-1 in (4.1), we get

$$a = \sqrt{1+hQ_w/Q_o} = \sqrt{1+hV_w/V_o} \tag{4.2}$$

This formula is made more important by experiments which show that h is constant in up flow and fast flow.

In Figure 4.2 we have plotted the volume where $\Omega_o/\Omega=H_o/L$, $L=H_o+H_w$, where $\Omega=\Omega_o+\Omega_w=\pi R_2^2(H_o+H_w)$ is the total volume, against the input flow ratio $Q_o/Q_w=V_o/V_w$. We can fit the data for up flow closely to the empirical curve

$$\frac{H_o}{L} = 1 - 1/(1+0.72V_o/V_w) \tag{4.3}$$

Hence $H_w/\Omega=1/(1+0.72V_o/V_w)$ and

$$H = \frac{Q_o}{Q_w}\frac{\Omega_w}{\Omega_o} = \frac{V_o}{V_w}\frac{H_w}{H_o} = 1/0.72 \tag{4.4}$$

This shows that h is constant in up flow of cylinder oil in water and is independent of any input ratio or flow condition.

Figure 4.3 is for down flow. The data points are more scattered in down than in up flow, especially for moderate input ratios. The empirical formula (4.3) which works for up flow does not work as well in down flow. The difference between up flow and down flow is more clearly expressed in figure 4.4.

One major conclusion implied by the data shown in figures 4.2 and 4.4 is that the holdup ratio h in *up flow* does not depend on the flow rates of oil and water or on the ratio of flow rates. The holdup ratio in *down flow* depends strongly on these parameters, as is shown in figures 4.3 and 4.4. These figures show that when the flow rates are large the effects of gravity are suppressed, as are the differences between up and down flow. Hence in fast flows the holdup ratios are the same and equal to approximately 1.39 in both up and down flow. This result agrees with conventional wisdom, the water is being held up, but disagrees with results of Charles, Govier and Hodgson [1961] (hereinafter as CGH) who found that in horizontal pipes, when the densities of oil and water are matched, the holdup ratio does depend on the input ratio and flow velocity, even at large flow rates.

Figure 4.1 Long oil slug suspended by gravity in down flow of water when the water flow rate is about 0.04 ft./sec. The slug is fluidized, in equilibrium under weight and drag. The holdup ratio is zero. Transient traveling spiral waves, called corkscrews, can be seen on different segments of the core. It is easy to fluidize much longer slugs, even to have a continuous core of oil fill the entire down flow pipe.

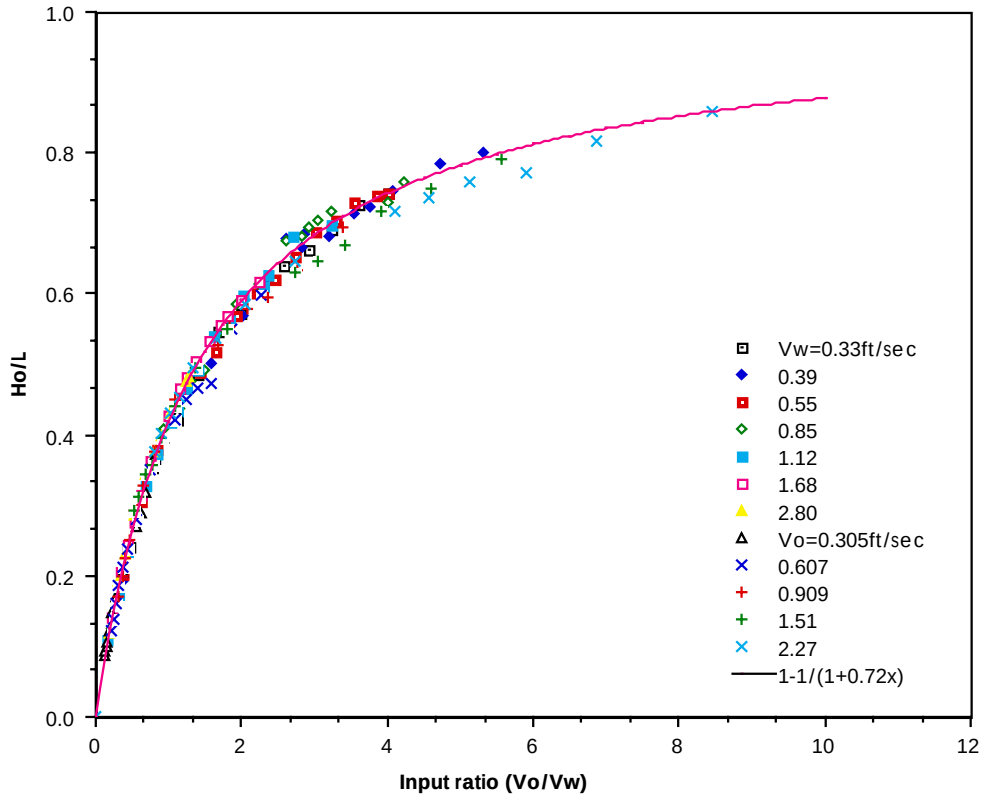

Figure 4.2 The volume ratio Ωo/Ω=Ho/L versus the input ratio Vo/Vw for up flow . The data falls close to the solid line given by (4.3). The data points are given by the superficial velocity of water Vw in ft/sec.

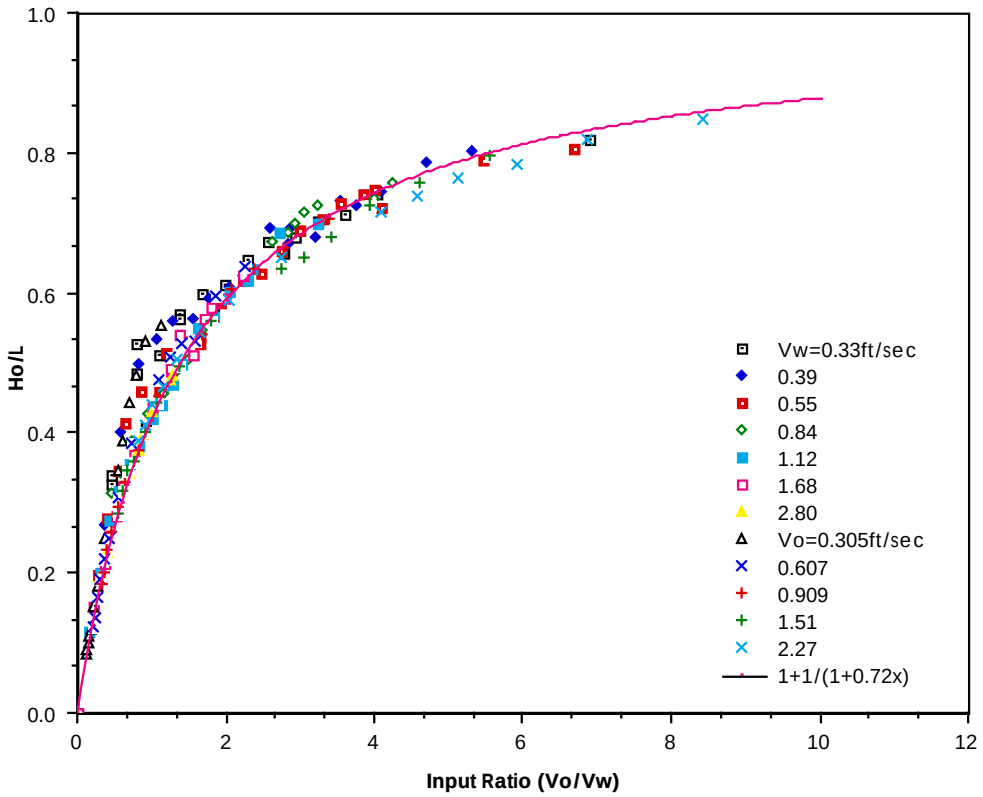

Figure 4.3 The volume ratio versus input ratio for down flow. The formula (4.3) is plotted. The data points are designated as in Figure 4.3.

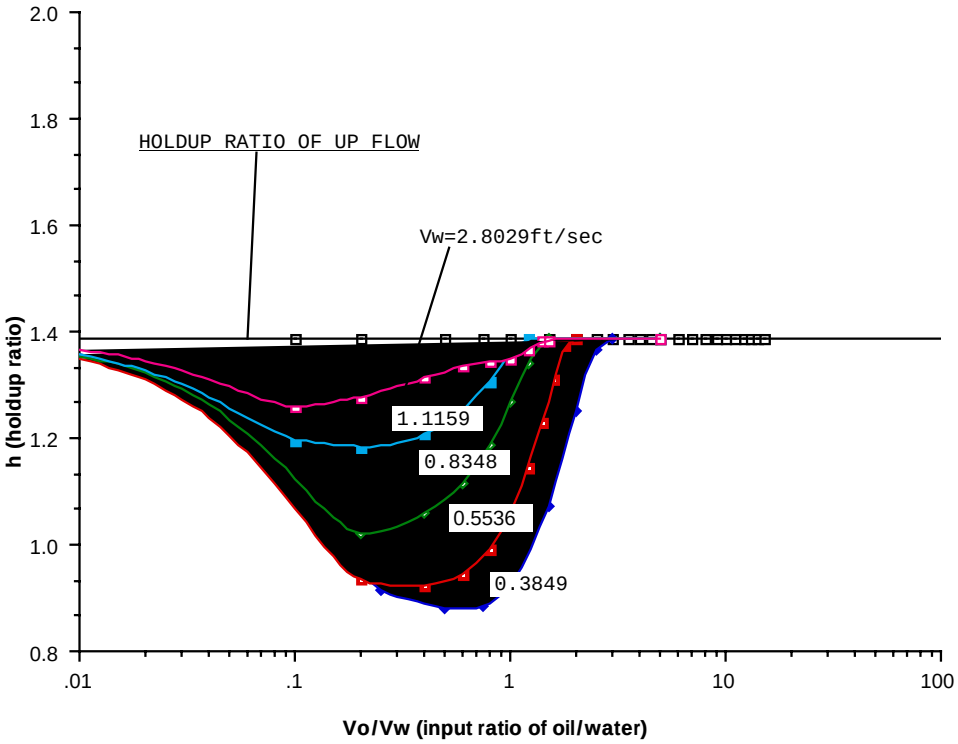

Figure 4.4 Holdup ratio in down flow as a function of Vo/Vw with Vw as a parameter.

5. Flow types

About six or seven qualitatively different flow regimes can be distinguished in experiments. There is some subjectivity involved in the delineation of differences which might be labeled qualitative or merely quantitative, so that the exact number of qualitatively different regimes may differ slightly from observer to observer. The flow regimes which appear in horizontal pipes under conditions of matched density have been already identified in the paper by CGH who studied concurrent flow of water and oil-carbon tetrachloride solution in a 1.04 in diameter pipe. Some of the different regimes observed by them were studied theoretically by PCJ, HJ and CBJ. Many of the regimes of flow identified by CGH and some new ones, for example, bamboo waves, appear in vertical flow. We were not able to study the important regime in which water emulsifies into the oil, called "water droplets" by CGH, because our apparatus is not strong enough to withstand the high pressure gradients generated in this condition in which water lubrication fails.

In this section we shall give a qualitative description of the types of flow we encounter, together with illustrative photographs and a discussion of some underlying physical mechanisms associated with the different flow types. Different types of flow are associated with different regions on a flow chart whose coordinates may be chosen as the superficial velocities of oil and water. The disposition of the flow types on the flow chart is considered in §6.

(i) Oil bubbles in water. These bubbles arise from capillary instabilities in the presence of shear. Oil bubbles in water are produced by capillarity but the size of the bubbles is determined by other factors, like shear, as well. The range of sizes of the bubbles which are observed is fairly well predicted by the linear theory of stability using Rayleigh's idea that the size of the bubble which will be observed corresponds to one-half of the length of maximum growth. Of course, in the present case, shear flow has a strong influence on the length of maximum growth. PCJ investigated this idea by comparing calculations from the linear theory of stability with the size of bubbles observed in the experiments of CGH. Their results, reported in their Table 1, show good agreement.

As a rule of thumb, we can say that we will always have oil bubbles in water if there is a large amount of water. Dispersions of oil in water, rather than bubbles, appear when the water velocity is much larger than the oil velocity. Dispersions will be discussed under (vii) below.

There is a marked difference in the distribution of bubbles in up flow and in down flow, even when they are of approximately the same size. In up flow the bubbles tend to spread and distribute themselves uniformly in the pipe. The wake interactions are weak because the velocity of the oil relative to the water is small. The oil is lifted by gravity relative to a forced stream of water moving in the same direction. Bubbles in down flow tend to aggregate. Wake forces between bubbles in down flow are much greater than in up flow because the bubbles are lifted against the forced stream of water, producing larger relative velocities and stronger wakes.

The tendency of bubbles to disperse in up flow and to aggregate in down flow is evident in the photograph shown in figure 5.1.

(a) (b)

Figure 5.1 Oil bubbles in water.

(a) Up flow. The bubbles do not aggregate. Wake forces are weak.

(b) Down flow. Bubbles aggregate in bubbles trains held together by wake forces.

(ii) Slugs of oil in water. If an oil bubble in water has a natural diameter larger than the pipe diameter, it will not fit in the pipe. One way to get the entire volume into the pipe is to squash it into a capsule shape. These capsule shapes are dynamically possible because they are shear stabilized by water. They move through the pipe freely lubricated on all sides by water in a manner reminiscent of capsule transport in pneumatic tubes.

Slugs form readily from bubble aggregates in down flow when the oil fraction is increased. The bubble aggregates collapse to form longer slugs which have a relatively large diameter lubricated by a thin layer of water. Long slugs are like segments of PCAF, but they support corkscrew waves. Corkscrew waves look like a periodically buckled wimpy rod which rotates in the water due to hydrodynamic torques. Corkscrew waves on a long shear stabilized slug are shown in figure 4.1 and many of them can be seen in the down flow side on the right of photographs shown in figure 9, say 9.4.

It seems to be impossible to create capsule slugs and corkscrew waves in up flow. In up flow bubbles don't aggregate to form slugs as the oil input is increased. Instead filaments are pulled out, the bubbles are stretched, as shown in the photograph of figure 5.2, under the combined action of buoyancy and lubrication forces described in the caption of figure 5.5. This filamentation gives rise to the bamboo waves which are described next.

(a) (b)

Figure 5.2 Oil slugs in water.

(a) Up flow. The larger bubbles are stretched out under the action of shear and buoyancy. This is shear stabilization of slugs and bubbles leading to long bamboo waves.

(b) Down flows. The oil is held up by buoyancy and slugs held together by wakes forming long trains.

(iii) Bamboo waves (BW). The shear stabilization of capillary instabilities in up flow leads to a regime of wavy flow in trains of sharp crests connected by long filaments. We call these bamboo waves. Superficially they resemble Stokes waves except that they perturb a cylinder and are imperfect. Many photographs of bamboo waves under different conditions are shown in the photographs of §9. The filaments which connect the crests thicken as the oil velocity V_o is increased for a fixed V_w and the average length of a wave decreases. These effects are evident in the photographs exhibited in figure 5.3 and are documented in the graphs of data assembled in figure 5.4. These waves are nearly stationary in a coordinate system moving with the undisturbed interface velocity so that the wave speed relative to laboratory coordinates also increases with increasing oil input.

Bamboo waves are a very robust regime of up flow, occupying a large area in the up flow charts shown in figures 6.1 through 6.4. They seem to maintain well-defined average wave lengths and wave speeds, but they are imperfect. The overtaking of one crest by another and the transient stretching of filaments between the waves is a frequent occurrence.

Bamboo waves in up flow are stretched due to the combined action of buoyancy and lubrication forces. The buoyancy part of this mechanism is simply that the oil is lifted by gravity relative to the heavy water which in any event is stationary on the pipe wall. The crest of a wave on the oil must move forward relative to the water. We noted already that the wave is nearly stationary, convected with the oil, unable to move fast on the oil core because the oil is so viscous. This means that there will be a positive buildup of pressure on the up side and a decrease of pressure on the down side of every crest in up flow, as shown in figure 5.5 The pressure associated with this lubrication effect will induce stretching in the same sense as buoyancy, elongating the wave, stretching the stems. On the other hand, the effects of buoyancy and lubrication are opposed in down flow. This tends to compress, even to eliminate bamboo waves and may lead to the form of buckling which we have called corkscrew.

Figure 5.3 Thin and thick bamboo waves. The bamboo thickens and the average length of a wave decreases when the oil velocity increases a fixed value of the water velocity. Some very short bamboo waves associated with high input velocities are shown in figure 5.6.

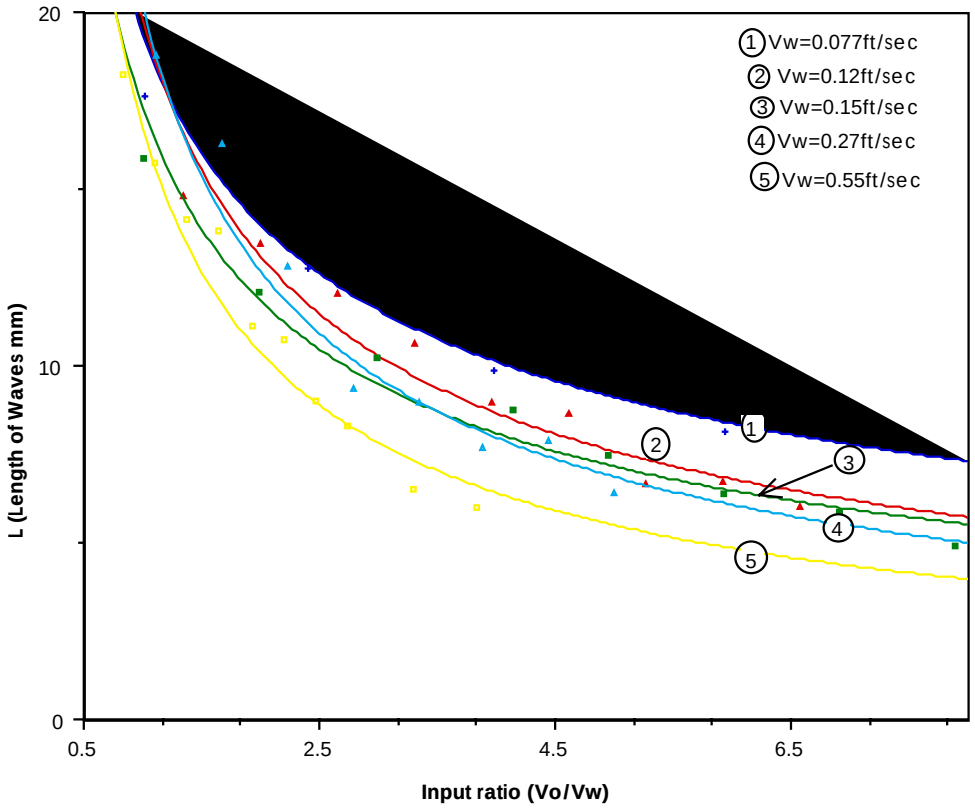

Figure 5.4 The average length of a bamboo wave decreases monotonically as the oil input is increase for fixed flow rate of water.

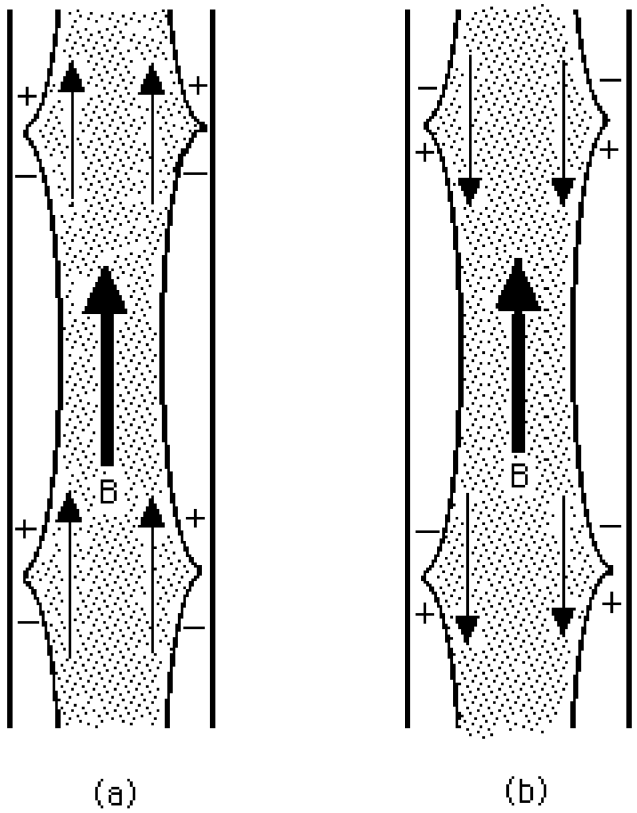

Figure 5.5 Lubrication forces arise from bamboo waves which in the first approximation are connected with the oil relative to stationary walls. The pressures which develop in the water in the front and back of crests are designated by (+-) and buoyancy of oil relative to water are designated by B. The pressure forces and buoyancy work together in up flow (a) where they lead to stretching and are opposed in down flow (b) where they lead compression and buckling.

(iv) Disturbed bamboo waves (DBW). We have already mentioned that when the driving pressure gradients are relatively large and the flow is fast, the differences between up and down flow vanish. In particular, the asymmetric effects of buoyancy on the holdup ratio are relatively less important when the pressure gradients are large. This can be seen in the disturbed up and down flow bamboo waves shown in figure 5.6. Some effects of buoyancy on the wave lengths are still in evidence, with stretched waves in up flow and compressed ones in down flow. At a lower speed, the up flow waves would elongate and the bamboo stems would thin, while in down flow the stems thicken into columns of oil which support perfect core annular flow which is perturbed by corkscrew waves from place to place. At faster speed the oil core cannot keep its integrity and various kinds of dispersions of oil in water and water in oil will form.

(a) (b)

Figure 5.6 Disturbed bamboo waves. When the pressure gradients are much larger than buoyancy, the difference between up flow (a) and down flow (b) is suppressed. One sees short, thick-stemmed waves. The effects of stretching in up flow and compression in down flow are still active in producing longer waves in up flow.

(v) Disturbed core annular flow (DCAF) and corkscrew waves. Perfect core annular flow (PCAF) is the basic flow whose stability was studied in the references mentioned in the introduction. In PCAF the core has a perfectly cylindrical interface of uniform radius which is perfectly centered on the pipe axis with an annulus of lubricating water outside. Good photographs of PCAF are shown in figures of CBJ. Figures 9.1–9.9 of this paper show PCAF disturbed by transient spiral waves which we call corkscrew. We call this regime of flow disturbed core-annular flow (DCAF). Actually, the motion of a corkscrew as it is screwed forward in the cork is an accurate description of the waves we see. These waves are not understood by us but they are perhaps associated with the buckling of a very soft rubber when loaded with shear tractions, which in our experiments are generated by the motion of water in the annulus. The apparent velocity of advance of the turning corkscrew is larger than the superficial velocity of oil or water. When the water flow rate is fixed in the small to moderate range where corkscrew waves appear, the pitch of the screw will increase with increasing rates of flow of oil leading to an apparent slowing of the wave. In this way one can obtain a nearly perfect core annular flow.

Figure 5.7 Disturbed core annular flow (DCAF). Some portions of the oil column in down flow are nearly perfect (a) while others are buckled and rotate as a corkscrew (b).

(vi) Oils sticks to the wall. The glass wall of the pipe is wet preferentially by water. However, when the water flow rate is small and the oil flow is large, oil can displace the water on the wall of the pipe. This usually happens first in up flow. At still higher values of the oil flow rate, water will disperse or emulsify into oil. This dispersion is discussed under (vii) below.

The deposition of oil on the pipe wall can sometimes be observed as a slow propagation of the wetting front with oil on the wall behind the front and water on the

wall before the front. We call this phenomenon "chugging." Two chugging configurations in up flow are exhibited in figure 5.8. To achieve chugging we increase the oil flow rate, keeping the water rate constant. In (a) and (b) an oil core plus oil bubbles are ejected from the sheath of oil on the wall. Evidently there is an annulus of water between the sheath and the core. There is a blockage when the oil seizes the wall which is relieved by an oil core-water annulus-oil sheath configuration. Shearing forces tear away many oil bubbles which form a cloud around an oil core in (a), more clearly seen in (b). If the oil flow rate is increased further, more oil bubbles than in (a) will be formed followed by a phase inversion in which water droplets emulsify and oil becomes the continuous phase. This leads to a loss of lubrication and to huge increases in the pressure gradient.

The fact that oil replaces water on a hydrophilic wall under certain repeatable dynamical conditions is of wide interest because the complete solution of the problem of wetting and spreading cannot be solved by thermodynamic and generalized energy considerations; it is not only a problem of finding good constitutive models. The answer to the question "When two fluids flow, which one will be on the wall?" depends on the history of the motion as well as the properties and interactions of the two fluids and the wall.

In figure 5.9 we see that oil may be deposited or removed from the hydrophilic glass pipe. In figure 5.10 the oil is deposited on one part of the glass wall, water on the other. Joseph, Singh and Chen [1990] showed how you could get oil to absorb on the plexiglass wall of a Taylor apparatus at the

downflow cell boundary of a Taylor cell of an emulsified oil, but not elsewhere. This "painted" configuration of absorption remains "forever" even after the motion is put to rest. People who actually work for a living know they have to wash their hands to get them clean.

CGH got water lubrication for three different oils, 6.29, 16.8 and 65.0 centipoise, in a 1.04" cellulose acetate-butyrate pipe which is *hydrophobic*. This shows that water lubrication is mainly a dynamical effect, with a secondary role played by wettability. To more fully understand this we need to consider the problem of *phase inversion* which is considered in the next subsection.

Hasson, Mann and Nir [1970] studied core flow of water in a heavier (1.02 gm/cm^3 organic liquid (kerosene-perchlorthylene solution). They didn't know that their flow is unstable because the organic solution has a higher viscosity. Their pipe was of glass, preferentially wet by water, and they studied film rupture. They say that

> The mechanism whereby the preferentially wall-wetting core liquid causes film rupture is not sufficiently clear. Accidental wetting of the glass wall by water is apparently insufficient in itself to disintegrate the organic film. The observed reproducibility in the break-up location (Figure 8) in spite of the wavy interface and the occasional water drops adhering to the pipe wall, suggests that the criterion governing the occurrence of film rupture must also involve a film momentum resisting break-up. It may be of significance that break-up film-thicknesses measured from enlarged photographs for the data plotted in Figure 8, were all roughly equal. The mean value of the break-up thickness was 500 micron, with a random scatter in the range of 300 to 700 micron while the interfacial velocities in the vicinity of the break-up point were of the order of 20 cm/sec.

(a) (b)

Figure 5.8 Deposition of oil on the wall. Oil seizes the hydrophilic glass wall when the oil flow rate is increased at a small fixed water flow rate (see "oil sticks to the wall" on the flow charts in §6). After the oil seizes the wall, the pipe is blocked and the blockage is relieved by an oil core-water-annulus-oil sheath configuration.

(a) A bubble cloud around an internal core.

(b) A clearer picture of the ejected core.

(a) (b)

Figure 5.9 (a) Removal of oil from the hydrophilic wall in down flow. Look at the bottom of the photograph. Oil is being removed from the wall. Slugs and bubbles are entering the oil sheath where they are lubricated by water.

(b) Oil is deposited on the wall in down flow. Slugs and bubbles are ejected from the sheath.

(a) (b)

Figure 5.10 Some oil sticks on the wall, water flowing through. In a static tube filled with water one can see stationary slugs of oil clinging to the wall which don't move even though they are buoyed up.

(vii) Dispersions. Phase inversion. There is evidently a dispersion limit in which large bubbles, slugs, sheets, and other coherent bodies of a single fluid are broken up by forces associated with the motion. A dispersion of immiscible liquids, one of which is polar, the other non-polar, is often called an oil and water dispersion or emulsion. An emulsion is a stable dispersion, but stability here is defined in a time frame so that a dispersion over a long time can be considered an emulsion over a short time. There are water in oil (w/o) dispersions and oil in water dispersions (o/w). There are conditions under which an o/w dispersion will change to w/o dispersion. This is called a phase inversion. It is also possible for o/w and w/o dispersions to coexist. The formation of dispersions, their natural properties, phase inversion may be studied in different systems; CGH give some data for dispersions in core annular flow of oil and water. Joseph, Singh and Chen [1990] have studied dispersions of oil and water and dispersions of silicone and vegetable oil in a Taylor-Couette apparatus.

Dispersions will always form in motions of two immiscible liquids which are sufficiently intense. CGH gave data for the formation of dispersions; w/o dispersions were called "water drops in oil" and o/w dispersions were called "oil drops in water." Generally a drop is heavier than the host fluid and in this sense the phrase "oil drops in water" is a misnomer.

This distinction between small bubbles of oil in water and o/w dispersions can be fuzzy. PCJ calculated the size of a small bubble which would arise in the experiment of CGH on "oil drops in water." The computed size was 4/3 the size of the largest oil bubble in the dispersion. The other bubbles in the dispersion were much smaller. Perhaps the study of equilibrium of the size of single drops and bubbles in different flows is fundamental in distinguishing between bubbles and dispersions.

The o/w dispersions are a lubricated regime of flow, which is of interest since they burn with reduced NO_X and particulate emissions.

We could not emulsify oil into water with our apparatus. Water in oil dispersions have a higher viscosity than oil alone; lubrication is lost and the resulting pressure gradients are greater than the

apparatus could withstand. The w/o dispersions have higher oil flow rates than the one in which oil seizes the wall. If we tried to increase the flow of oil in a case like that in figure 5.1a, the pressure gradient would shoot up. We think if we could run the apparatus at the high pressure, a phase inversion to a w/o dispersion would result. The w/o dispersions and phase inversion from o/w dispersions are dangerous because they destroy lubrication.

CGH gave three flow charts for 6.29, 16.8 and 65 cp oils. They identified a phase inversion boundary in the region of dispersions. This boundary does not seem to depend strongly on the properties of the viscosity or interfacial tension but the water fraction is important. They observed w/o dispersions for water fractions ranging from 10 to 67% at sufficiently high oil velocities. In laboratory and field tests, Charles [1960] reports that

> Very substantial reductions in pressure gradient are again evident. For water contents up to about 20 per cent the pressure gradient was affected very little by the addition of the water and these conditions probably correspond to the water-in-oil emulsion flow pattern. At a water content of approximately 20 per cent a sudden decrease in pressure gradient was observed which was probably coincident with the transition of the flow pattern to stratified flow. For water contents greater than 40 per cent the pressure gradient was reduced by factors in excess of 10. The results obtained with the field pipeline indicted that optimum reduction of pressure gradients was obtained when the water was added to the extent of 30 to 50 per cent of the total liquid flow.

Topological considerations, like the packing fractions of monodisperse and polydisperse spheres, are of importance in emulsion rheology and are probably important for the problem of the phase inversion of dispersions in lubricated pipelining. The rhomboidal packing point for monosized spheres is the closest possible packing of spheres and the volume fraction of sphere in this packing is 74.08%. Imagine that we have a dispersion of monosized spheres of oil; for example, many spheres of oil are shown in figure 5.8(a), but they are polydisperse. A monodisperse dispersion of such oil spheres could not exist if the water fraction was less than 25.92% because there would be no room for the oil spheres. Either we get polydisperse oil spheres, sphere distortions which are energetically unstable, or phase inversions.

6. Flow charts

A flow chart is a graph in the (V_W, V_O) plane in which regions of different flow types are designated. The holdup ratio h for each (V_W, V_O) point may be obtained from figure 4.4 and the corresponding value of the water fraction given by $a=R_2/R_1$ from (4.4). The determination of a for a given (V_W, V_O) is simplified by the fact that h=1.38 universally in up flow and for fast down flows.

In figure 6.1 we have plotted a chart showing the flow type of an emulsified oil of viscosity near 5 poise in up flow of 0.4% aqueous sodium silicate solution. The flow condition is identified by points in the (V_W, V_O) plane, where $V_W=Q_W/A$ is the superficial velocity of the water and V_O is the superficial velocity of the oil.

In figure 6.2 we plotted a flow chart for up flow using the same oil with pure water in a freshly cleaned pipe.

Figure 6.3 is a flow chart for down flow under the condition specified in figure 6.1. Figure 6.4 is the down flow chart using fresh water in a freshly cleaned pipe.

The figures may be compared with the flow charts of CGH. The flow types are not the same; they did not have bamboo waves or disturbed core annular flow with corkscrew waves and we could achieve the pressure gradients necessary for emulsification of water into oil. Nevertheless, the interested reader will find the way to identify similar regimes. The regularity with which flow types fall on flow charts is gratifying.

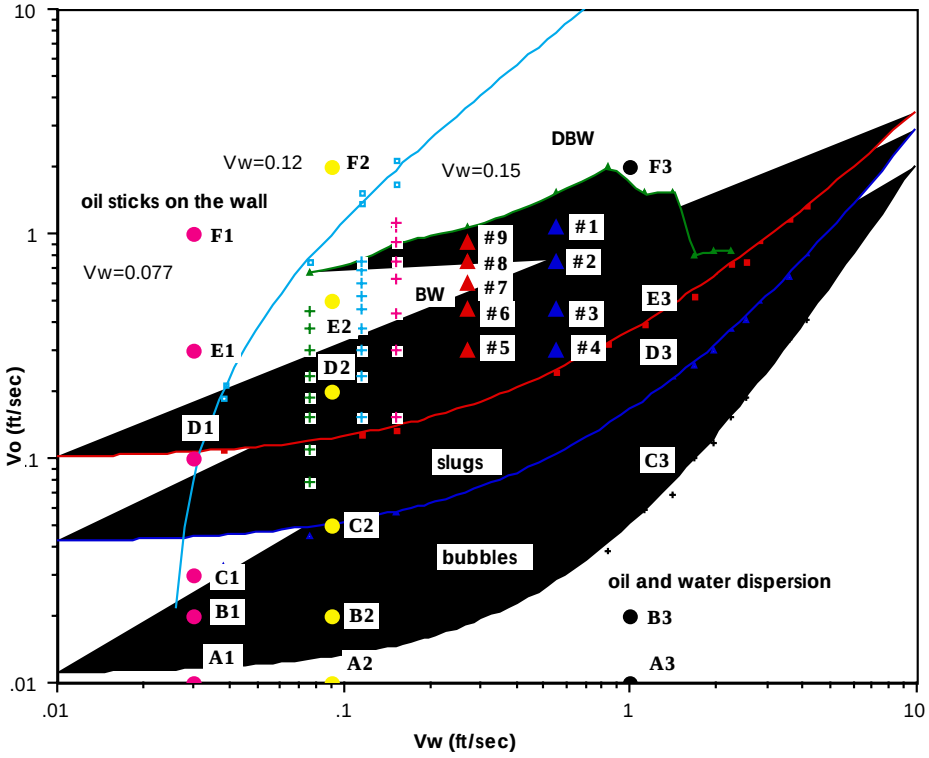

Figure 6.1 Flow condition in up flow as a function of the superficial water (with sodium silicate) velocity $V_W=Q_W/A$ and oil velocity $V_o=Q_o/A$. The holdup ratio is universally h=1.38 (see figure 4.4) and the value of $a=R_2/R_1$ can be obtained from (4.2) for each and every point. The labeled circles and triangles are calculated are identified for comparison with theory in §9.

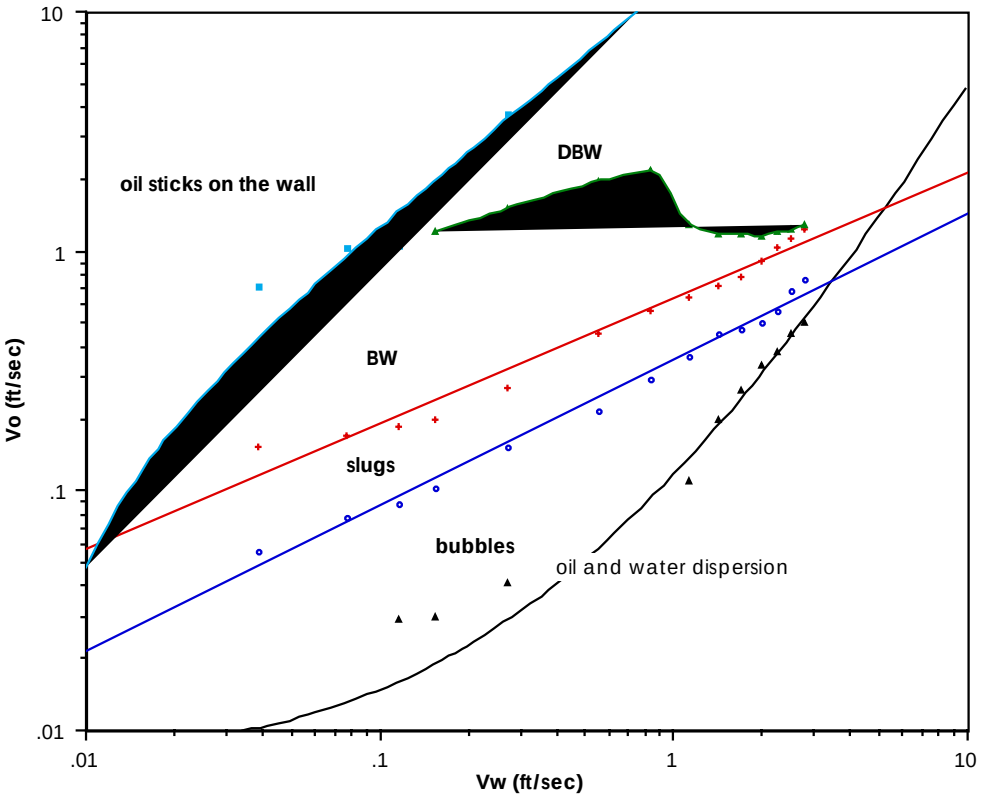

Figure 6.2 Flow chart in up flow as in 5.1 except that fresh water is used in a freshly cleaned pipe. There is a small upward shift probably due to a decrease in the water fraction, h=1.38 for this flow.

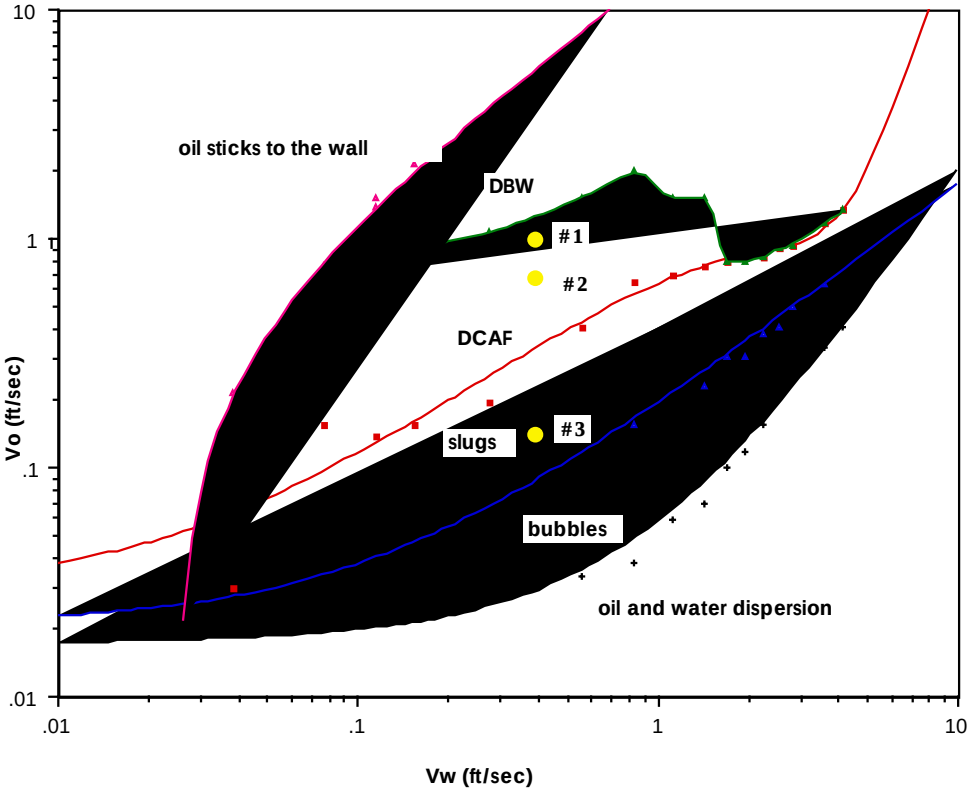

Figure 6.3 Flow condition in down flow as a function of the superficial velocities. The value of $a=R_2/R_1$ can be determined from (4.2) when the holdup ratio h is given by experiment as in Figure 4.4. Disturbance in disturbed core annular flow (DCAF) are corkscrew waves near the slugs boundary and immature bamboo waves near the DBW boundary. The three circles are computed points. The linear theory of stability is discussed in §9.

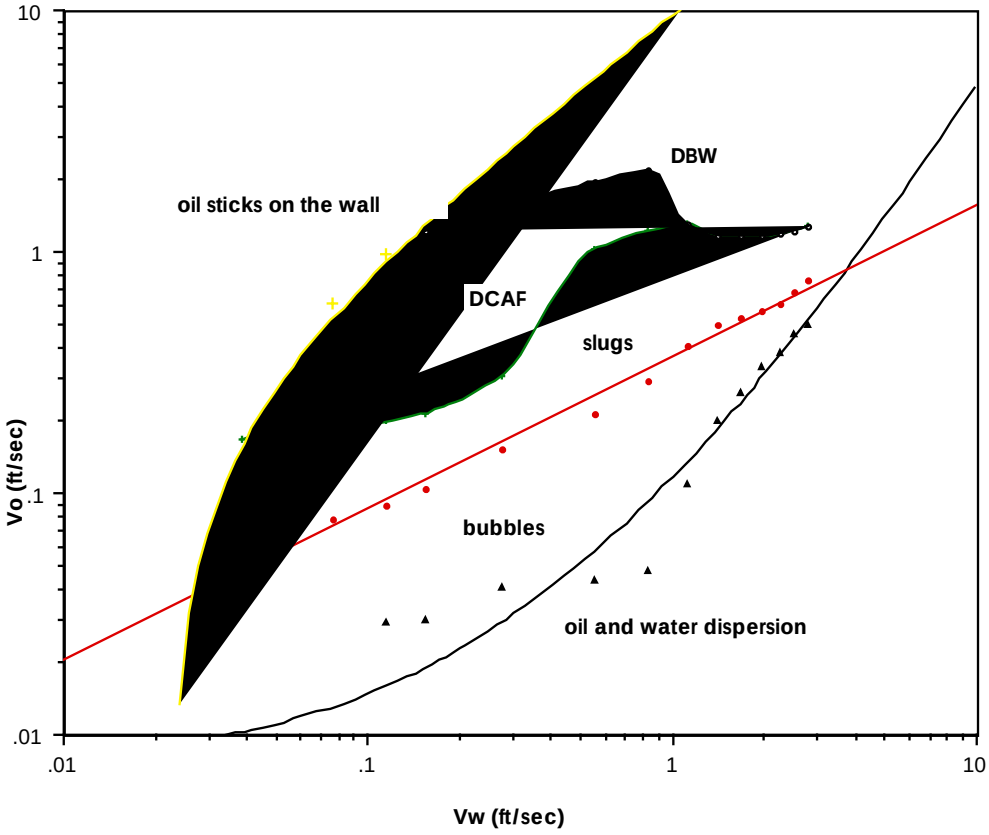

Figure 6.4 Flow chart for down flow using fresh water in a newly cleaned pipe.

7. Pressure drop measurements

Data on pressure drops and holdup ratios were obtained for different flow rates of oil and water. We are expressing the flow rates Qw, Qo in terms of superficial velocities (Vw, Vo) = (Qw, Qo)/A in ft/sec where $A=\pi d^2/4$ and d=3/8 inch. Data was taken for six values of Vw = .329, .385, .554, .834, 1.116, 1.678, 2.803 and five values of Vo = .305, .607, .909, 1.513 and 2.269. We fix Vw (or Vo) and take measurements for all Vo (or Vw). We measure Δp for motion by manometer measurements using equations (3.6) and (3.7). The pressure gradient due to motion is $\Delta p/L$. We define a dimensionless pressure gradient

$$\Theta = \Delta p/\rho_w gL \tag{7.1}$$

which is expressed as feet of water/foot. Measured values of the pressure drop vs. the flow rate ratio with V_w as a parameter are given in figure 7.1.

Measured values of the pressure drop vs. the flow rate ratio with Vo as a parameter are given in figure 7.2. The reader's attention should focus on the following practical result: for a fixed flow rate of oil there is an optimal flow rate Vw of water, with Vw/Vo between 0.2 and 0.8 in the experiments, for which Θ is minimum. This means the flow rates of water and oil can be adjusted to minimize energy expenditure while transporting the same amount of oil. The minimum Θ point moves toward lower values of Vw/Vo as Vo is increased. All the minimum points in up flow are located in regions of bamboo waves. The minimum pressure gradients fall in the region of disturbed core annular flow. In this region one finds corkscrew waves, perfect or nearly perfect core annular flow with disturbance in the form of immature corkscrew waves, or bamboo waves.

In figure 7.3 we compare the pressure gradients in up flow and down flow as a function of the input ratio. The difference in the pressure gradients depends mainly on the rate of flow of lubricating water. For high pressure gradients the effects of buoyancy are relatively small and the differences between up and down flow are suppressed. In general the pressure gradients in down flow are smaller

because of the effects of buoyancy which lead to greater accumulations of oil and more energy efficient flow regimes in down flow.

The manner in which the oil is introduced into the pipe has some effect on the pressure drops. We did some testing of the effect of the diameter of the nozzle used to introduce the oil centrally in the pipe. In figure 7.4 we have compared two nozzles. The large nozzle has a nominal inside diameter of 0.2". The smaller nozzle has a nominal inside diameter of 0.17". The smaller nozzles were rejected because they give rise to higher pressure gradients, especially when oil flow rates are large. The reason is that when the nozzle is small, for one reason or another many small oil bubbles are formed at the exit lip. Although the flow will soon tend to a steady state compatible with a particular set of operating conditions, the small bubbles persist and produce an additional pressure drop. This effect is greatly enhanced by increasing the flow rate of oil.

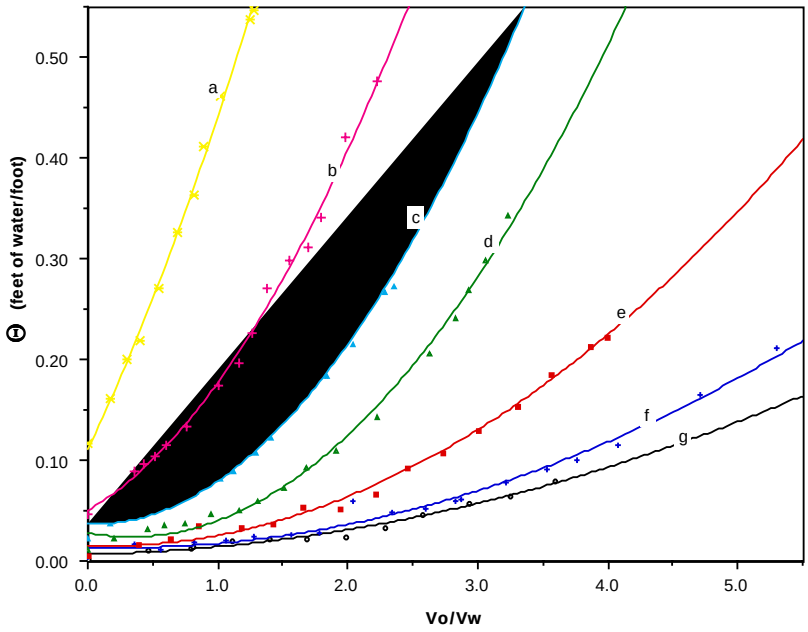

Figure7.1(a)

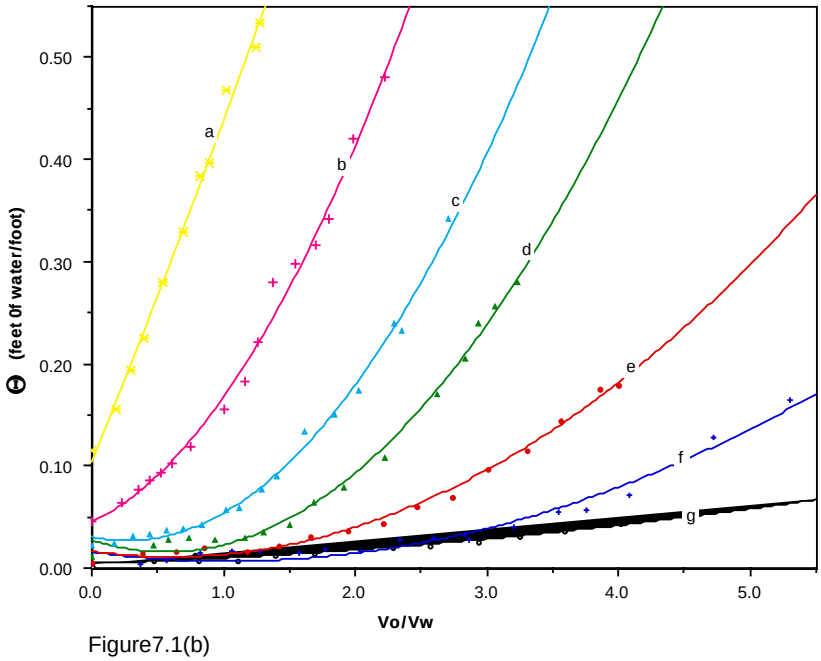

Figure7.1(b)

Figure 7.1 Pressure drop per unit length as a function of the input ratio for various values of water flow velocity Vw in ft/sec: (a) 2.80, (b) 1.08, (c) 1.12, (d) 0.83, (e) 0.55, (f) 0.38, (g) 0.33. For each Vw, Θ is an increasing function of Vo, with larger increases for larger values of Vw and no increases, even decreases, for small value of Vw. (a) up flow, (b) down flow.

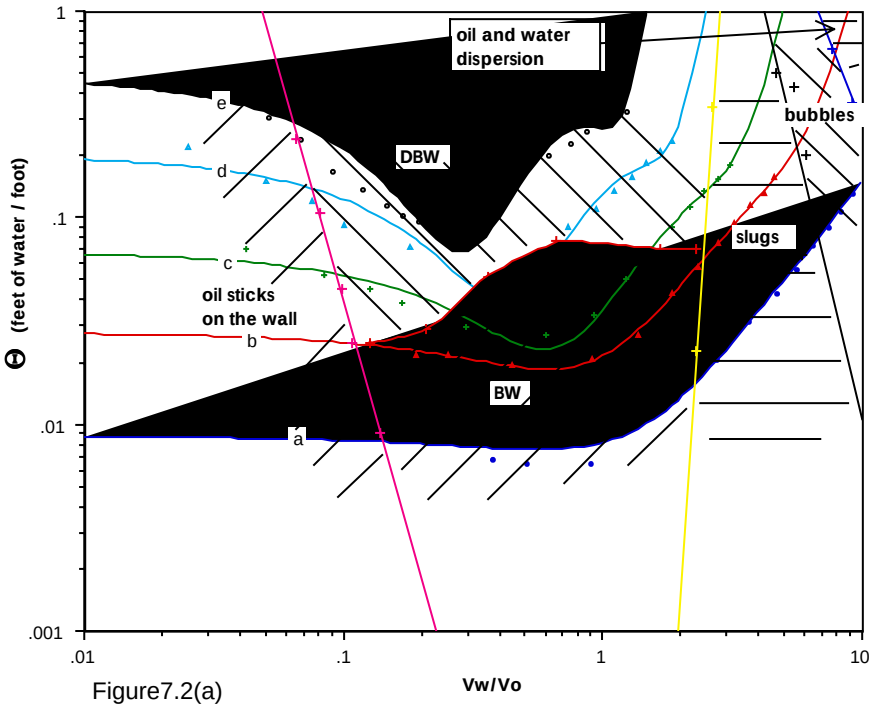

Figure7.2(a)

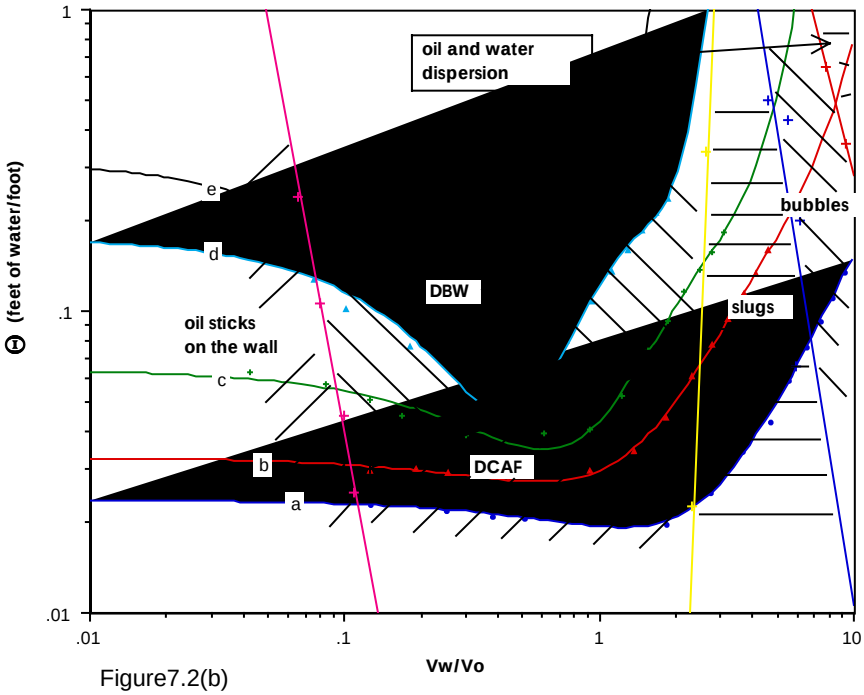

Figure7.2(b)

Figure 7.2 Dimensionless pressure gradient versus the inverse input ratio for different values of the oil velocity in ft/sec: (a) 0.31, (b) 0.61, (c) 0.91, (d) 1.51, (e) 2.27. (a) up flow, (b) down flow.

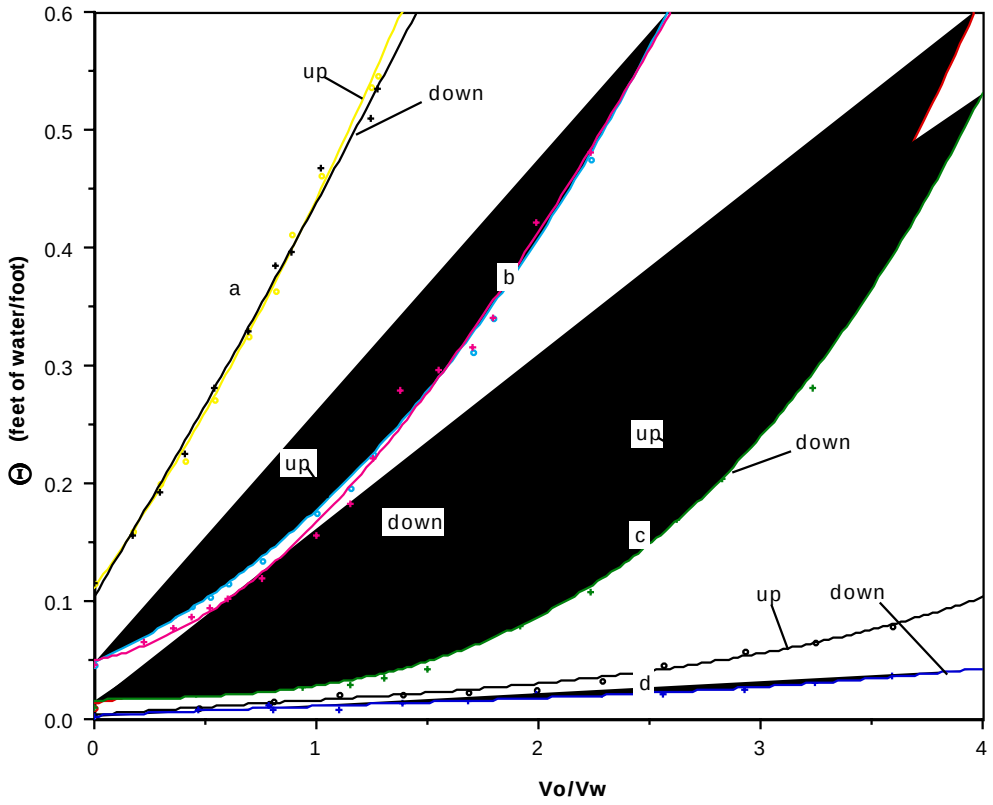

Figure 7.3 Comparison of the pressure drop per unit length as a function of the input ratio for four values of Vw in ft/sec: (a) 2.80, (b) 1.68, (c) 0.83, (d) 0.33.

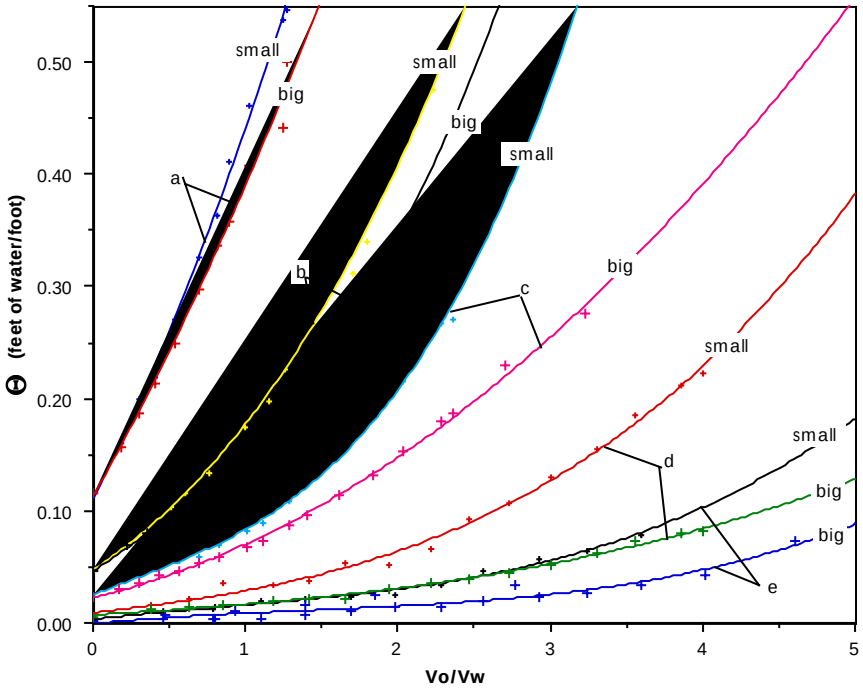

Figure7.4(a)

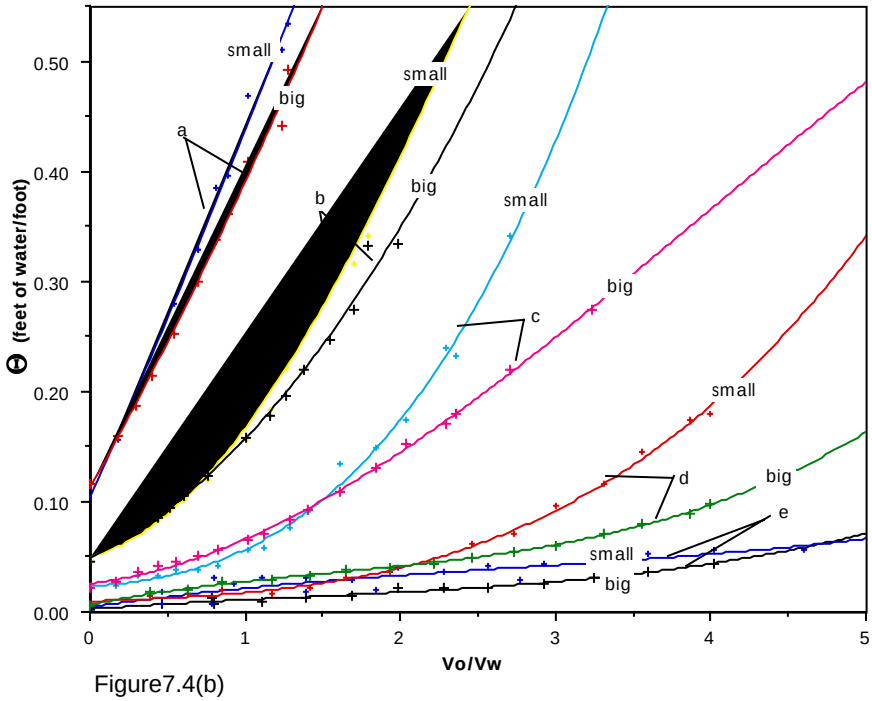

Figure7.4(b)

Figure 7.4 The effect of the nozzle diameter on the pressure drop as a function of the input ratio for different values of the water velocity Vw in ft/sec: (a) 2.80, (b) 1.68, (c) 1.12, (d) 0.55, (e) 0.33. The nozzle "big" has an inside diameter of 0.2, "small" has an inside diameter of 0.17. (a) up flow, (b) down flow.

8. Ideal and measured efficiency of water lubrication

To assess the energy saving due to water lubrication in vertical flow, we compared measured values of the flow rates, holdup ratio and pressure gradients with certain ideal values computed in different ways which are described below. The ideal values are determined by the solutions of the equations

$$O = -\hat{P}' + \rho_l\, g + \mu_l \left(W'' + \frac{1}{r} W' \right) = 0 \tag{8.1}$$

for $W=W_l(r)$ which holds for up flow in the region $l=1$ of the core $0<r<R_1$ and the region $l=2$ of the annulus $R_1<r<R_2$ (see CBJ) when

$$\frac{d\hat{P}_1}{dx} = \frac{d\hat{P}_2}{dx} = \hat{P}'$$

is one and the same constant pressure gradient.

To compare this ideal flow with experiments, we must remove the part of the pressure associated with the composite density of the mixture

$$\rho_c = \frac{\rho_w Hw + \rho_o Ho}{Hw+Ho}$$

where L=Ho+Hw and Ho, Hw are the heights of the oil and water in the pipeline which were introduced in §3. We may determine Ho and Hw in terms of $\eta=1/a=R_1/R_2$ and L by the conservation of volume

$$Ho\pi R_2^2 = \pi R_1^2 L\,,$$
$$Hw\pi R_2^2 = \pi(R_2^2 - R_1^2)L\,.$$

Hence

$$Ho = \eta^2 L,\ Hw = (1-\eta^2)L \tag{8.2}$$

and

$$\rho_c = (1-\eta^2)\rho_2 + \eta^2\rho_1 \tag{8.3}$$

where $\rho_2=\rho_w$ and $\rho_1=\rho_o$.

The dynamic pressure p which we measure by the method of §3 is then given by

$$\hat{P} = p + \rho_c g x$$

and

$$-\hat{P}' + \rho_1 g = -p' + (\rho_1 - \rho_c) g \tag{8.4}$$

where, using (8.3), we find that

$$\rho_1 - \rho_c = (1-\eta^2)\,\hat{u}\rho\hat{o}\,,$$
$$\rho_2 - \rho_c = -\eta^2\,\hat{u}\rho\hat{o}\,. \tag{8.5}$$

Then, we have

$$-p' + (1-\eta^2)\,\hat{u}\rho\hat{o}\, g + \mu_1 \left(W'' + \frac{1}{r} W'\right) = 0\,,\ 0 \le r \le R_1\,,$$
$$-p' - \eta^2\,\hat{u}\rho\hat{o}\, g + \mu_2 \left(W'' + \frac{1}{r} W'\right) = 0\,,\ R_1 \le r \le R_2\,. \tag{8.6}$$

Equations (8.6) show that core annular flow in a vertical pipe depends on the density through the density difference and only through the density difference. These terms disappear entirely from the governing equation (8.5) when the flow is all oil, $\eta=1$, or all water, $\eta=0$.

If we think of x increasing in the same direction as the pressure drop, we have the same equation (8.5) in down flow but with gravity reversed. The equations derived below are for up flow. To get the equations for down flow, change the sign of g.

The solution of (8.6) together with appropriate boundary and interface conditions stated by CBJ is

$$W_1 = \frac{f_1}{4\mu_1}\,(R_1^2 - r^2) + \frac{f_2}{4\mu_2}\,(R_2^2 - r_1^2) + \frac{R_1^2 \hat{u}\rho\hat{o}g}{2\mu_2}\,\ln\frac{R_2}{R_1} \tag{8.7}$$

where

$$f_1 = -p' + (1-\eta^2)\,\hat{u}\rho\hat{o}g$$
$$f_2 = -p' - \eta^2\,\hat{u}\rho\hat{o}g \tag{8.8}$$

in up flow and

$$W_2(r) = \frac{f_2}{4\mu_2}(R_2^2 - r^2) - \frac{R_1^2 \hat{u}\rho\hat{o}g}{2\mu_2}\,\ln\frac{r}{R_2}\ . \tag{8.9}$$

The oil flow rate is given by

$$Q_1 = 2\pi \int_0^{R_1} r W_1(r)\,dr =$$
$$2\pi\left\{\frac{f_1}{16\mu_1}R_1^4 + \frac{f_2}{8\mu_2}\,(R_2^2R_1^2 - R_1^4) + \frac{R_1^4\hat{u}\rho\hat{o}g}{4\mu_2}\,\ln\frac{R_2}{R_1}\right\}\ . \tag{8.10}$$

The water flow rate is given by

$$Q_2 = 2\pi \int_{R_1}^{R_2} r W_2(r)\,dr =$$
$$2\pi\left\{\frac{f_2}{16\mu_2}(R_2^2 - R_1^2)^2 + \frac{\hat{u}\rho\hat{o}g}{8\mu_2}\left[R_1^2R_2^2 + 2R_1^4\,\ln\frac{R_1}{R_2} - R_1^4\right]\right\}\ . \tag{8.11}$$

When there is all oil in the pipe $R_1=R_2$, $Q_2=0$, $f_1=p'$. When there is all water in the pipe $R_1=0$ and $Q_1=0$, $f_2= -p'$. Hence in both cases

$$Q = -\frac{p'}{8\mu}\,\pi R_2^4\ . \tag{8.12}$$

When g=0, the case of matched densities studied by CGH, we have

$$Q_1 = -\frac{p'\pi R_1^4}{8\mu_1}\left\{1 + 2\frac{\mu_1}{\mu_2}\left(\frac{R_2^2}{R_1^2} - 1\right)\right\} \tag{8.13}$$

and

$$Q_2 = \frac{-p'\pi}{16\mu_2}\,(R_2^2 - R_1^2)^2 \tag{8.14}$$

We may define various optimization problems using the formulas. For example, JRR found the water fraction, the value of R_1 such that the total volume flux Q_1+Q_2 is maximum among all the flows satisfying (8.13) and (8.14) for a given pressure gradient p'. Another problem is to maximize Q_1 alone under the same conditions. This is a payoff calculation in which the water fraction is chosen to maximize the throughput of oil. This problem was solved when $\hat{u}\rho\hat{o}g=0$ by Russell and Charles [1959] and their solution was derived again by Joseph, Nguyen and Beavers [1984].

The slightly more difficult case of vertical flow is considered below. First we rewrite (8.10) and (8.11) in a more convenient form in which we introduce the superficial velocities $V_o=Q_1/\pi R_2^2$ and $V_w=Q_2/\pi R_2^2$. Thus

$$\begin{aligned}\frac{4V_o\mu_2}{R_2^2 g} &= \frac{-p'}{g}\left\{\frac{m}{2}\eta^4 + \eta^2 - \eta^4\right\} \\ &\quad + \hat{u}\rho\hat{o}\left\{\frac{m}{2}(\eta^4 - \eta^6) - \eta^4 + \eta^6 - 2\eta^4 \ln\eta\right\}\end{aligned} \tag{8.15}$$

and

$$\frac{4V_w\mu_2}{R_2^2 g} = -\frac{p'}{2g}(1-\eta^2)^2 + \hat{u}\rho\hat{o}\,\{\,\eta^4 - \eta^6 + 4\eta^4 \ln\eta\} \tag{8.16}$$

Equations (8.15) and (8.16) each depend on two dimensionless parameters and the right side of both depends on one parameter $p'/g\hat{u}\rho\hat{o}$ which is positive $p'<0$, $\hat{u}\rho\hat{o}<0$ in our flows. The same formulas hold in down flow with the sign of g reversed.

A theoretical formula for the holdup ratio can be derived from (4.1), (8.2), (8.15) and (8.16)

$$h = V_o H_w / V_w H_o = \frac{(1-\eta^2)\left\{\Theta\left(\frac{m}{2}\eta^4+\eta^2-\eta^4\right)+\frac{\hat{u}\rho\hat{o}}{\rho_w}\left[\left(\frac{m}{2}-1\right)(\eta^4-\eta^6)-2\eta^4 l n\eta\right]\right\}}{\eta^2\left\{\Theta(1-\eta^2)^2+\frac{\hat{u}\rho\hat{o}}{\rho_w}(\eta^4-\eta^6+4\eta^4 l n\eta)\right\}} \tag{8.17}$$

where

$$\frac{-p'}{\rho_w g} \overset{\text{def}}{=} \Theta \tag{8.18}$$

is a dimensionless pressure gradient which can be compared with $\Delta p/\rho_w gL$ measured in experiments.

The maximization problem solved by Russel and Charles [1959] is to maximize V_o with respect to η, for fixed p' when $\hat{u}\rho\hat{o}$. They found that V_o is maximum when

$$\eta = \left(\frac{1}{2-m}\right)^{1/2}.$$

In our experiments

$m \spadesuit 1/601'', \hat{u}\rho\hat{o}g = -0.090g$

and the oil flow-pressure gradient relation (8.15) for up flow becomes

$$\frac{4V_o\mu_2}{R_2^2 g\rho_w} = -\frac{p'}{g\rho_w}(\eta^2-\eta^4) - \frac{0.090}{\rho_w}(\eta^6-\eta^4-2\eta^4 l n\eta) \tag{8.19}$$

where ρ_w=0.995, to within a small error. The same formula holds in down flow with the sign of g reversed.

In the first five rows of table 8.1 we compare experimental and ideal results for five cases of up flow, and in rows 6 through 10 for five cases of down flow. The columns of this table are as follows: V_{oe} is the superficial velocity from experiments, V_we the prescribed water velocity, h_e is the holdup ratio from figure 4.4, $\eta_e = R_{1e}/R_2$ is the experimental ratio of the mean radius of the interface to pipe radius

which is computed from h_e, using (4.4), and Θ_e is the measured value of dimensionless pressure gradient. We may define an ideal flow as PCAF satisfying (8.15) and (8.16). Then η, $\Theta_L(\eta)$ are computed from (8.15) and (8.16) when $(V_o,V_w) = (V_{oe},V_{we})$ and (8.17) determines $h_L(\eta)$. $\Theta_L(\eta_e)$, $V_{WL}(\eta_e)$ and $h_L(\eta_e)$ are computed from the formulas when $(\eta, V_o) = (\eta_e, V_{oe})$ are given. The value $\eta=1/\sqrt{2}$ is a good approximation to the value of η which minimizes $\Theta(\eta)= -p'/g\rho_w$ for a fixed value of V_o. We can prove this when η is close to one by noting that

$$\begin{aligned}\eta^6 - \eta^4 - 2\eta^4 \ln\eta &= \eta^6 - \eta^4 - \eta^4 \ln[1-(1-\eta^2)] \\ &= \eta^6 - \eta^4 + \eta^4(1-\eta^2) + O[(1-\eta^2)^2] \\ &= O[(1-\eta^2)^2] \end{aligned} \tag{8.20}$$

The result $\eta=1/\sqrt{2}$ follows from (8.19) when the second term of the right hand side is zero. $\eta_m(\Theta_e)$ is the value of η which maximizes $V_O = V_{OL}(\Theta_e)$ in (8.15) when $\Theta = \Theta_e$ and $h_L(\eta_m)$ is calculated from (8.17) with $(\eta, \Theta) = (\eta_m, \Theta_e)$.

The value $\Theta(1)$ is the dimensionless pressure gradient required to transport oil alone in the same pipe with the same oil throughput. We obtain

$$\Theta(1) = 8V_o\mu_1/gR_2^2\rho_w \tag{8.21}$$

from (8.15) with $\eta=1$.

Another measure of efficiency which is used in the oil industry is to compare the observed pressure gradient Θ_e with the pressure drop $\Theta(0)$ required to transport water alone with a volume flux $Q_{o+w} = Q_o+Q_w$ equal to the total flux. We can compute $\Theta_L(0)$ for the laminar flow of water from (8.12)

$$\Theta_L(0) = \frac{8V_{o+w}\mu_2}{gR_2^2\rho_w} \text{ (laminar)} \tag{8.22}$$

where $V_{o+w}=V_o+V_{we}=Q_{o+w}/A$ can be obtained from tables.

In table 8.2 we have various pressure gradient ratios, which are measures of efficiency together with the values of the Reynolds number

$$\leftarrow e = \frac{V_{o+w} d}{\nu_w} \quad , \nu_w = \mu_2/\rho_w$$

where d=3/8 in and $\mu_2=10^{-2}$ poise. Hence

$$\leftarrow e = V_{o+w} \frac{12(2.54)^2 300}{8} \cong 2903\ V_{o+w} \tag{8.23}$$

For Re>2300 we should not compare Θ_e with $\Theta_L(0)$ for laminar flow. For these, we should compute $\Theta_T(0)$, the pressure gradient required to transport water at a superficial velocity of V_{o+w}. It requires a greater pressure gradient, $\Theta_T(0)=k\Theta_L(0)$ with k>1; for example, k=3/2, to transport a given mass flux in turbulent flow. So as a rough measure the reader should reduce the number $\Theta_L(0)/\Theta_c$ by 2/3 when Re>2300. In this way we may understand the statement that it can happen that the pressure gradient required to drive oil plus water in the lubricated pipeline, can be smaller than the pressure gradient required to drive the same flux of water alone.

From our comparisons of ideal and measured values of the pressure gradients we may draw the following conclusions.

- The pressure drops required to transport a given flux of oil with water lubrication are more than 100 times less than pressure drops required to transport the same flux of 601 cp oil without lubrication. In general, in vertical pipes we expect reduction of the order k/m where $m=\mu_2/\mu_1$ and k is a fraction, say about 1/5.

- The pressure drops required to transport a given flux of oil and water with water lubrication is about the same, of the same order, and can be even less than the pressure drop necessary to transport water alone at a superficial velocity V_{o+w} corresponding to the total flux provided that V_{o+w} is such that $\leftarrow e$ given by (8.23) is greater than 2300. In this case the pressure drop in the water alone is computed for turbulent flow.

- Bamboo waves require a much greater pressure gradient to transport a given volume flux of oil at low oil velocity and fixed water velocity than in the ideal case. This comparison is not interesting because its significance is diminished by the fact that oil is usually being transported by buoyancy.

- Disturbed core annular flow with corkscrew waves is energy efficient, with pressure gradients only moderately greater, sometimes even less than those required for perfect core annular flow with the same water fraction. This shows that DCAF is close to PCAF.

	Voe	Vwe	η_e	flow type	he	Θ_e	η	$\Theta_L(\eta)$	$h_L(\eta)$
1.	0.305	0.554	0.53	BW	1.39	0.019	0.34	0.0013	4.18
2.	0.607	0.272	0.77	BW	1.39	0.020	0.56	-0.004	4.83
3.	0.909	0.554	0.80	BW	1.39	0.027	0.58	0.003	3.31
4.	1.513	0.445	0.83	BW	1.39	0.052	0.72	0.016	2.53
5.	2.269	0.494	0.88	DBW	1.39	0.096	0.82	0.044	2.19
6.	0.305	0.554	0.59	DCAF	1.39	0.020	0.61	0.026	1.59
7.	0.607	0.154	0.85	DCAF	1.39	0.025	0.85	0.028	1.59
8.	0.909	0.154	0.80	DCAF	1.39	0.033	0.88	0.038	1.78
9.	1.513	0.554	0.83	DCAF	1.39	0.052	0.78	0.050	1.72
10.	2.269	0.554	0.86	DBW	1.39	0.090	0.83	0.071	1.86

	$Q_L(\eta_e)$	$V_{wL}(\eta_e)$	$h_L(\eta_e)$	$\eta_m(\Theta_e)$	$V_{oL}(\Theta_e)$	$V_{wL}(\Theta_e)$	$h_L(\eta_m)$	$\Theta_L(1)$	$\Theta_L(o)$
1.	-0.011	-0.046*	-16.7	0.67	1.68	0.82	2.53	2.34	.0095
2.	-0.00013	0.11	3.89	0.67	1.73	0.84	2.51	4.65	.0097
3.	0.0038	0.25	2.97	0.67	2.04	1.01	2.41	6.96	.016
4.	0.026	0.31	2.29	0.68	3.17	1.60	2.24	11.6	.023
5.	0.062	0.31	2.11	0.69	5.16	2.61	2.141	7.4	.031
6.	0.027	0.64	0.91	0.89	0.34	0.06	1.55	2.34	.0095
7.	0.028	0.14	1.61	0.86	0.50	0.11	1.57	4.65	.0084
8.	0.04	0.12	1.84	0.82	0.81	0.24	1.62	6.96	.012
9.	0.051	0.45	1.76	0.77	1.61	0.65	1.72	11.6	.023
10.	0.076	0.41	1.90	0.74	3.31	1.53	1.84	17.4	.031

Table 8.1 Comparision of experimental and ideal values in up flow (#1-5) and down flow (#6-10) for the same oil flow. V is given in ft/sec. The other quantities are dimensionless. *The velocity profile for this case of negative V_w is shown in figure 8.1.

	flow type	$\Theta_{L(1)}/\Theta_e$	$\Theta_{L(\eta)}/\Theta_e$	$\Theta_{L(\eta_e)}/\Theta_e$	$\Theta_{L(o)}/\Theta_e$	R
1.	BW	122.93	0.068	-0.58	0.49	2481
2.	BW	232.46	-0.20	-0.0065	0.49	2599
3.	BW	257.88	0.11	0.14	0.60	4226
4.	BW	222.87	0.31	0.50	0.44	5656
5.	DBW	180.97	0.46	0.65	0.32	7981
6.	DCAF	116.79	1.30	1.35	0.47	2481
7.	DCAF	185.97	1.12	1.12	0.34	2198
8.	DCAF	210.99	0.85	1.21	0.36	3071
9.	DCAF	222.88	0.96	0.98	0.44	5971
10.	DBW	193.04	0.79	1.07	0.35	8155

Table 8.2 Comparison of the ratio of ideal to the experimental pressure gradients for the same oil flow. The Reynolds number $R=(V_o+V_w)d/\nu_w$. $R>R_c$ where $R_c \bullet 2000$, the flow is turbulent. In the turbulent case we should replace $\Theta_{L(o)}$ with $\Theta_{T(o)}>\Theta_{L(o)}$ because a greater pressure gradient is required for the same volume flux in turbulence flow.

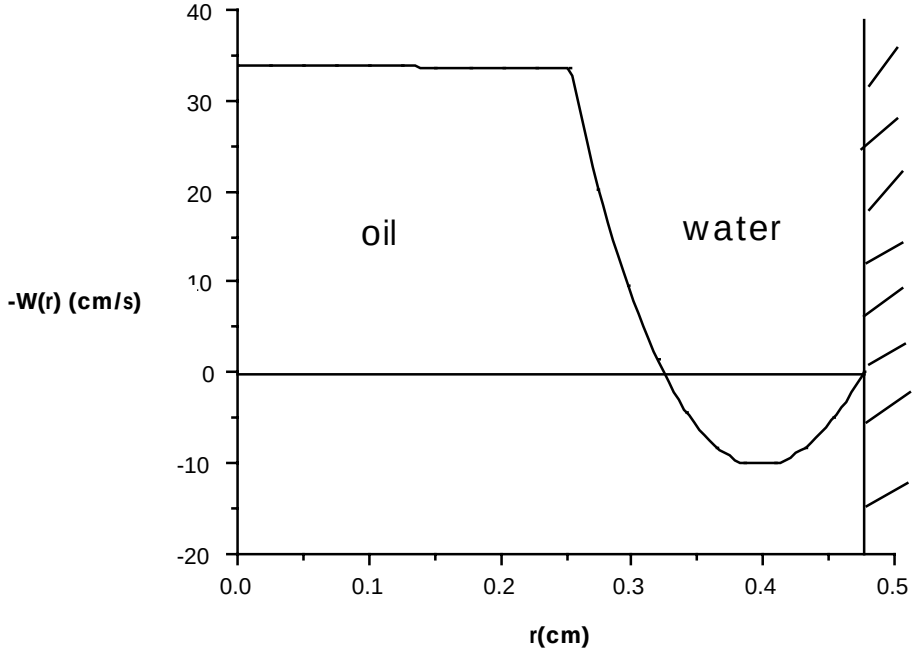

Figure 8.1 Up flow with negative flow of water, $V_o = 0.305$ ft/sec, $V_w = -0.046$ ft/sec.

9. Comparison of experiments with the linear theory of stability

We computed results from the linear theory of stability using the equations of CBJ. The Reynolds number used by CBJ is defined as $\leftarrow_{g}^{(R_1)} = WgR_1/\nu_1$ where $Wg=gR_1^2/\nu_1$ and $F= -\hat{P}'/\rho_1 g$. Lengths are scaled with R_1, velocity with Wg and time with $R_1/|Wg|$. CBJ took x increasing in the direction of gravity so that W(r) in up flow in this paper is –W(r) in CBJ.

We did two kinds of comparisons of theory and experiments. First, we calculated wave lengths and wave speeds in the regions of parameter space in which waves were observed and compared the calculated and measured values. Second, we tried to determine the regions of parameter space where different flow types could be found by analysis of the energy of the most dangerous disturbance.

It is useful here to draw attention again to the fact that we are trying to compare results of a linear theory of stability of PCAF with flow types in deeply nonlinear regions of flow. There are different ways to make this comparison corresponding to different choices of the laminar flow which is supposed to be relevant for the nonlinear flow which is observed. We shall give a more precise characterization of the possible choices below.

A laminar flow is determined by two parameters, say V_w and V_o or V_o and $a=1/\eta=R_2/R_1$ or V_w and a. For example, given V_o and V_w we may compute η and p' from (8.15) and (8.16). We may conclude that other types of flow, say bamboo waves, are determined by prescribing two parameters plus the flow type. We are going to choose to make our comparisons for all flow types having

1) the same oil and water inputs; that is, V_o and V_w are prescribed and equal to measured values

2) the same oil input, V_o and the same water fraction expressed by $a=a_e$ where a_e is taken from the measured holdup $h=h_e$ in figure 4.4. Bamboo waves trap water between the creases (see figure 5.5) and sweep it through the system faster than

in laminar flow: less water is held up. The $\eta_e > \eta$ or $a_e < a$ in up flow. In down flow this trapping does not operate and the experimental holdup is nearly the same as the laminar one (see table 8.1).

(i) Comparison of linear theory with experiments for fixed values of V_o and V_w

Calculations were carried out for the emulsified oil used in the experiments at a temperature of 22° with material parameters given by (2.1). The dimensionless parameters which can be computed from the parameters given by (2.1) are

$$m = 1/601,\ \rho_w/\rho_o = 0.995/0.905 = 1.10\ ,\ \ J^* = \frac{TR_2}{\rho_o \nu_o^2} = 0.102\ . \tag{9.1}$$

In our first comparison of linear theory with experiments, we select nine arbitrary cases of bamboo waves from experiments and compare observed and calculated wave lengths and wave speeds. Bamboo waves are imperfectly periodic but it is easy to identify average values, taken as simple averages from video recordings using scaled reticle and automatic lapsed-timer features. To compute wave lengths and wave speed from linear theory, we need to identify the unstable wave of maximum growth. For this we need to prescribe dimensionless parameters a, F and ←g which can be obtained from PCAF formulas in §8; values of the oil and water volume flow rates $Q_o=V_o/A$ and $Q_w=V_w/A$ are prescribed. The values of these parameters at the labeled flow points in the chart of figure 6.1 are listed in table 9.1.

(ia) Up flow. The comparison of computed and measured values of the wave speed and wave length of bamboo waves for points 1 through 9 of figure 6.1 is given in table 9.2. The measured values of the wave length are on the average slightly larger than computed values, probably due to the nonlinear stretching associated with the lubrication and buoyancy effects described in figure 5.5.

The speed W(1) of the undisturbed interface is on the average slightly larger than the computed value of c. This shows that the bamboo wave is on the average basically stationary in a frame moving with velocity W(1). As a further check we computed c=8.03, W(1)=9.84 at point D2 and c=16.96, W(1)=18.95 at E2. The viscosity of the oil is too large to support any but slowly propagating waves, so the wave is convected with the oil. Analysis of the singular problem m∅0 by HLJ shows that c∅W(1) in the limit m∅0.

The discrepancy between the computed and measured values of the wave speed is consistent with the idea that the wave is convected with the oil. The reason for the discrepancy can be traced to the fact that the water fraction for laminar flow with V_o, V_w prescribed is larger than the measured water fraction in up flow; $\eta<\eta_e$ in the first five columns of table 8.1. Since V_o is prescribed, and the same value in laminar flow and bamboo waves, the oil in a core with $R_1<R_{1e}$ must flow faster. Hence the speed discrepancy between c in theory and experiments is due to the reduction of the water fraction due to sweep out effects of bamboo waves.

We turn next to analysis of the equation governing the evolution of the kinetic energy E of a disturbance of PCAF. This may be written as

$$\dot{E} = I–D + B1 + B2 + B3 \tag{9.1}$$

where I–D is the Reynolds stress minus the dissipation (and we normalize with D=1), B1 is a boundary term associated with interfacial tension, B2 is a boundary term associated with the viscosity difference which we call interfacial friction and B3 is a boundary term in the energy supply which is proportional to gravity times the jump in density. All the terms in (9.1) are derived and explicit formulas for them are

given by CBJ. HJ introduced the idea that different terms of the energy equation should be computed on the most dangerous disturbance to help in the diagnosis of the mechanism producing instability. Table 9.3 shows that bamboo waves are driven by interfacial friction, the other terms in the energy equation are stabilizing with an ever so slight destabilizing effect from interfacial tension in experiments 4 and 5.

Photographs of the nine cases considered in tables 9.2 and 9.3 are shown in figures 9.1 through 9.9. The close-up photograph is taken from the TV monitor and shows an actual frame used in constructing the average wave length and wave speed. The still photograph from a distance shows both the up flow bamboo waves and down flow disturbed core annular flow with corkscrew waves.

Terms of energy budget for the other labeled points in the up flow chart of figure 6.1 are displayed in table 9.4. In addition, we have given the value of the wave length $\hat{\lambda} = 2\pi/\hat{\alpha}$ of the fastest growing wave. PCJ showed that the length of the slugs and bubbles which are observed correlate well with $\hat{\lambda}/2$. We would not get this kind of agreement here, because the slugs are stretched and stringy due to buoyancy and shear (see figures 5.2, 9.4). We have a good agreement between theory and experiment with regard to selection of flow type in a sense which needs explanation. In all the entries the Reynolds stress term I–D is stabilizing. HJa showed that when the flow is unstable $\overset{\circ}{E} > 0$ and I–D>0 is destabilizing, all other terms negative, correlate with transitions to w/o (water into oil) emulsions, in the experiments of CGH and in field tests, using privileged data. We have no budget which should lead to w/o dispersions and none are observed. In every case where slugs, bubbles and o/w dispersions are observed, PCAF is unstable both to interfacial friction B1 and interfacial friction; the other terms are stabilizing. The size of the bubbles in the o/w dispersions is much smaller than $\hat{\lambda}/2$ and is probably associated with the breakup of large bubbles in shear flow.

The energy budgets for the cases of bamboo waves (BW) and disturbed bamboo waves (DBW) that are observed are all alike. The instability producing these waves is due to a strongly positive B, with all other effects stabilizing or at least only weakly destabilizing. Interfacial friction drives interfacial waves.

(ib) Down flow. For down flow, we reverse the sign of g. We are going to compare theory and experiment at four arbitrarily chosen points on the down flow chart in figure 6.4. The flows at points in the region DCAF are essentially PCAF as the theory predicts (see table 9.6) The point #4 in the region DBW is unstable to interfacial friction. The point #1 in the region of slugs is unstable also to interfacial tension. This gives perfect agreement at all four points.

We carried out a similar computation, with V_o, a_e prescribed, but with parameters appropriate to pure oil. We get good agreements between theory and experiments, see table 9.10 and 9.11, even though the oil used in the experiments is not the one used in the theory. In fact many results are insensitive to small changes of viscosity when the water fraction is fixed.

(ii) Comparison of linear theory with experiment for fixed values of V_o and a

We remarked that the discrepancy between the theoretical and measured values of c in table 9.2 was due to the sweeping out of trapped water between the crests of bamboo waves leading to a reduced water fraction. To check this idea, we decided to compute stability results when V_o is prescribed as in the experiment and $a=a_e$ is given by experiment. This idea is completely consistent with results shown in Table 9.8. The energy decomposition shown in Table 9.9 is also completely consistent with the idea that bamboo waves are produced by interfacial friction.

	Experiment		Basic flow (8.7), (8.9) with the same V_o, V_w				
	V_o(ft/sec)	V_w(ft/sec)	a	W_0(cm/sec)	W(1)(cm/sec)	$\leftarrow_g(R_1)$	F
1	1.06	0.55	1.61	83.91	83.69	0.5749	-1.067
2	0.76	0.55	1.90	83.90	83.73	0.3475	-1.0737
3	0.46	0.55	2.44	83.03	82.91	0.1646	-1.0835
4	0.31	0.55	2.93	80.03	79.94	0.0951	-1.0893
5	0.31	0.27	2.58	62.15	62.05	0.1390	-1.0807
6	0.46	0.27	2.11	61.83	61.69	0.2563	-1.0722
7	0.61	0.27	1.78	58.66	58.49	0.4262	-1.0635
8	0.76	0.27	1.54	54.78	54.58	0.6595	-1.0556
9	0.91	0.27	1.38	53.23	53.01	0.9045	-1.0509
A1	0.01	0.03	8.03	19.68	19.67	0.0046	-1.0969
B1	0.02	0.03	6.41	25.04	25.02	0.0091	-1.0953
C1	0.03	0.03	5.59	28.62	28.59	0.0137	-1.0940
D1	0.1	0.03	3.63	40.09	40.04	0.0504	-1.0869
E1	0.3	0.03	2.18	43.39	43.27	0.2327	-1.0690
F1	1.0	0.03	1.03	32.80	31.91	2.1952	-1.1127
A2	0.01	0.09	8.52	22.14	22.13	0.0039	-1.0980
B2	0.02	0.09	6.72	27.57	27.55	0.0079	-1.0965
C2	0.05	0.09	4.87	36.21	36.18	0.0207	-1.0931
D2	0.2	0.09	2.82	48.50	48.41	0.1071	-1.0808
E2	0.5	0.09	1.48	33.27	33.09	0.7472	-1.0459
F2	2.0	0.09	1.04	67.16	65.93	2.1045	-1.1605
A3	0.01	1.0	14.95	68.98	68.97	0.0007	-1.1108
B3	0.02	1.0	10.91	73.51	73.50	0.0018	-1.0509
C3	0.1	1.0	5.42	90.68	90.65	0.0151	-1.1063
D3	0.3	1.0	3.41	106.16	106.09	0.0607	-1.0996
E3	0.5	1.0	2.72	112.95	112.85	0.1190	-1.0943
F3	2.0	1.0	1.49	135.06	134.74	0.7292	-1.0832

Table 9.1 Specification of parameters used to calculate theoretical values from the linear theory of stability at the labeled flow points in the flow chart of figure 6.1.

	Experiments		Computations		
Exp. no.	λ (cm)	c (cm/sec)	λ (cm)	c(cm/sec)	W(1)(cm/sec)
1	1.21	57.70	0.82	79.84	83.69
2	1.31	43.28	0.92	80.21	83.73
3	1.41	35.65	1.22	79.76	82.91
4	1.22	27.81	1.65	77.00	79.94
5	1.374	19.16	1.56	58.91	62.05
6	1.79	22.90	1.23	58.12	61.69
7	1.34	28.22	1.05	54.80	58.49
8	1.17	31.06	0.95	50.85	54.58
9	0.90	36.25	0.86	49.38	53.01

Table 9.2 Comparison of computed and measured values of the wave speed c and wave length λ of bamboo waves at the flow points #1 through #9 of the flow chart in figure 6.1 for up flow. The speed W(1) of the undisturbed interface is also listed for convenience. The computations are for the most unstable mode.

Exp.no.	$\mathring{E}$	I-D	B1	B2	B3
1	0.1836	-0.7932	-0.01419	0.9944	-0.00359
2	0.2142	-0.7680	-0.01080	0.9983	-0.00544
3	0.2759	-0.7081	0	0.9950	-0.01123
4	0.3480	-0.6332	0.01423	0.9873	-0.02057
5	0.3837	-0.5869	0.00830	0.9800	-0.01781
6	0.3133	-0.6485	-0.00321	0.9754	-0.01062
7	0.2640	-0.6996	-0.00968	0.9802	-0.00700
8	0.2244	-0.7405	-0.01329	0.9833	-0.00514
9	0.1829	-0.7881	-0.01554	0.9903	-0.00378

Table 9.3 Energy budget for equation (9.1) evaluated on the most unstable mode at each of 9 labeled points in figure 6.1. Positive values of $\mathring{E}$ mean that PCAF is unstable.

Points	$\dot{E}$	I-D	B_1	B_2	B_3	$\hat{\lambda}$(cm)	Flow region in the chart
A1	0.2450	-0.8982	0.4145	0.7341	-0.0060	1.5519	O/W dispersion
B1	0.2852	-0.8791	0.2085	0.9702	-0.0148	1.7295	oil bubble
C1	0.3052	-0.8610	0.1362	1.0485	-0.0189	1.7833	oil bubble
D1	0.4116	-0.6853	0.0388	1.0816	-0.0237	1.8341	BW/slug
E1	0.4264	-0.5353	0.0011	0.9798	-0.0141	1.4624	oil sticks on the pipe wall
F1	0.0032	-0.9954	-0.0021	0.9978	-0.0001	0.2342	oil sticks on the pipe wall
A2	0.2291	-0.9038	0.4840	0.6532	-0.0053	1.5268	O/W dispersion
B2	0.2719	-0.8862	0.2387	0.9331	-0.0143	1.7116	oil bubble
C2	0.3424	-0.8050	0.0909	1.0806	-0.0243	1.9188	oil slug
D2	0.4566	-0.5449	0.0167	1.0068	-0.0220	1.7690	BW
E2	0.2814	-0.6791	-0.0120	0.9799	-0.0075	1.1267	BW
F2	0.0552	-0.9261	-0.0115	0.9968	-0.0001	0.2604	oil sticks on the pipe wall
A3	0.0742	-0.9778	1.1728	-0.1204	-0.0012	1.0009	O/W dispersion
B3	0.1353	-0.9530	0.7341	0.3618	-0.0084	1.3061	O/W dispersion
C3	0.2721	-0.8208	0.1095	1.0203	-0.0373	2.1226	oil bubble
D3	0.2983	-0.7031	0.0221	1.0022	-0.0231	1.6892	oil slug
E3	0.2457	-0.7436	0.0030	0.9980	-0.0119	1.2353	BW
F3	0.1371	-0.8506	-0.0158	1.0049	-0.0014	0.6096	DBW

Table 9.4 Energy budget for equation (9.1) evaluated on the most unstable mode at labeled points in figure 6.1. $\hat{\lambda}$ is the dimensional wave length based on the most unstable mode.

	Experiment		Basic flow (8.7), (8.9) with the same Vo, Vw				
	V_o(ft/sec)	V_w(ft/sec)	a	W_0(cm/sec)	W(1)(cm/sec)	$\leftarrow_g(R_1)$	F
1	0.105	0.40	1.59	10.70	10.82	0.5965	-1.0356
2	0.70	0.40	1.34	37.33	37.37	1.0010	-1.0094
3	1.0	0.40	1.27	49.38	49.36	1.1638	-0.9964
4	4.0	0.40	1.09	145.74	144.54	1.8480	-0.8288

Table 9.5 Specification of parameters used to calculate theoretical values from the linear theory of stability at the labeled flow points in the flow chart of figure 6.3.

Points	$\dot{E}$	I-D	B_1	B_2	B_3	$\hat{\lambda}$(cm)	Flow region in the chart
1	0.1690	-0.8327	0.0035	1.2220	-0.2238	13.4382	slugs
2			stable				DCAF
3			stable				DCAF
4	0.0854	-0.9105	-0.0126	1.0085	0.0002	0.2887	DBW

Table 9.6 Energy budget for equation (9.1) evaluated on the most unstable mode at labeled points in figure 6.3. $\hat{\lambda}$ is the dimensional wave length based on the most unstable mode.

	Experiment			Basic flow (8.7), (8.9) with the same V_o, a			
	V_o(ft/sec)	V_w(ft/sec)	a	W_0(cm/sec)	W(1)(cm/sec)	$\leftarrow_g(R_1)$	F
1	1.06	0.55	1.31	55.89	55.64	1.0592	-1.0510
2	0.76	0.55	1.42	46.44	46.24	0.8396	-1.0491
3	0.46	0.55	1.64	37.43	37.26	0.5452	-1.0530
4	0.31	0.55	1.88	32.80	32.66	0.3633	-1.0589
5	0.31	0.27	1.50	20.91	20.75	0.7156	-1.0422
6	0.46	0.27	1.35	25.53	25.35	0.9697	-1.0382
7	0.61	0.27	1.27	30.15	29.95	1.1605	-1.0377
8	0.76	0.27	1.22	34.75	34.53	1.3077	-1.0394
9	0.91	0.27	1.19	39.37	39.12	1.4242	-1.0428

Table 9.7 Specification of parameters used to calculate theoretical values from the linear theory of stability at the labeled flow points in the flow chart of figure 6.1.

	Experiments		Computations		
Exp. no.	λ (cm)	c (cm/sec)	λ (cm)	c(cm/sec)	W(1)(cm/sec)
1	1.21	57.70	0.79	52.02	55.64
2	1.31	43.28	0.96	42.54	46.24
3	1.41	35.65	1.22	33.51	37.26
4	1.22	27.81	1.33	29.42	32.66
5	1.374	19.16	1.25	17.94	20.75
6	1.79	22.90	1.16	22.17	25.35
7	1.34	28.22	1.02	26.68	29.95
8	1.17	31.06	0.87	31.33	34.53
9	0.90	36.25	0.79	35.71	39.12

Table 9.8 Comparison of computed and measured values of the wave speed c and wave length λ of bamboo waves at the flow points #1 through #9 of the flow chart in figure 6.1 for up flow when V_o, $a=a_e$ are prescribed. The speed W(1) of the undisturbed interface is also listed for convenience. The computations are for the most unstable mode.

Exp.no.	$\mathring{E}$	I-D	B1	B2	B3
1	0.1552	-0.8214	-0.01659	0.9961	-0.00284
2	0.2117	-0.7511	-0.01409	0.9818	-0.00497
3	0.3352	-0.6131	-0.00851	0.9659	-0.00915
4	0.4186	-0.5502	-0.00451	0.9848	-0.01150
5	0.3491	-0.6323	-0.01078	1.0013	-0.00918
6	0.2463	-0.7165	-0.01238	0.9828	-0.00772
7	0.1805	-0.7826	-0.01422	0.9829	-0.00558
8	0.1402	-0.8303	-0.01603	0.9902	-0.00371
9	0.1203	-0.8487	-0.01584	0.9876	-0.00271

Table 9.9 Energy budget for equation (9.1) evaluated on the most unstable mode at each of 9 labeled points in figure 6.1 when V_o, $a=a_e$ are prescribed. Positive values of $\mathring{E}$ mean that PCAF is unstable. The flows are all unstable to interfacial friction $B_2>0$ leading to bamboo waves.

	Experiment			Basic flow (8.7), (8.9) with the same V_o, a			
	V_o(ft/sec)	V_w(ft/sec)	a	W_0(cm/sec)	W(1)(cm/sec)	$\leftarrow_g(R_1)$	F
1	1.06	0.55	1.31	55.69	55.53	0.2043	-1.0577
2	0.76	0.55	1.42	45.67	45.52	0.1620	-1.0587
3	0.46	0.55	1.64	37.43	37.27	0.1052	-1.0668
4	0.31	0.55	1.88	32.83	32.69	0.0701	-1.0760
5	0.31	0.27	1.50	20.90	20.79	0.1381	-1.0541
6	0.46	0.27	1.35	25.41	25.30	0.1871	-1.0469
7	0.61	0.27	1.27	30.00	29.88	0.2239	-1.0443
8	0.76	0.27	1.22	34.59	34.46	0.2523	-1.0444
9	0.91	0.27	1.19	39.33	39.19	0.2748	-1.0464

Table 9.10 Specification of parameters used to calculate theoretical values from the linear theory of stability at the labeled flow points in the flow chart of figure 6.1 (pure oil).

	Experiments		Computations		
Exp. no.	λ (cm)	c (cm/sec)	λ (cm)	c(cm/sec)	W(1)(cm/sec)
1	1.21	57.70	1.13	51.90	
2	1.31	43.28	1.33	42.83	
3	1.41	35.65	1.60	33.81	
4	1.22	27.81	1.75	29.91	
5	1.374	19.16	1.64	18.14	
6	1.79	22.90	1.47	22.48	
7	1.34	28.22	1.37	23.36	
8	1.17	31.06	1.23	31.21	
9	0.90	36.25	1.10	35.66	

Table 9.11 Comparison of computed values for the oil (2.2) with experiments done with the values of (2.1).

Exp.no.	$\mathring{E}$	I-D	B1	B2	B3
1	0.1855	-0.7985	-0.0118	0.9991	-0.0033
2	0.2585	-0.7229	-0.0086	0.9950	-0.0051
3	0.4033	-0.5871	-0.0028	1.0010	-0.0075
4	0.3763	-0.6231	-0.0044	1.0862	-0.0054
5	0.3935	-0.6231	-0.0044	1.0283	-0.0074
6	0.2672	-0.7327	-0.0082	1.0142	-0.0061
7	0.2010	-0.7844	-0.0097	1.0003	-0.0053
8	0.1583	-0.8222	-0.0113	0.9959	-0.0041
9	0.1315	-0.8470	-0.0125	0.9940	-0.0031

Table 9.12 The energy budgets for the most unstable modes corresponding to the experiments, normalized with D=1.

(a)

(b)

Figure 9.1 Flow condition at #1 ($V_W V_O$) = (0.55, 1.06) ft/sec of figure 6.1.

(a) Bamboo waves in up flow on the left, and disturbed core annular flow with immature bamboo and corkscrew waves in down flow on the right.

(b) Bamboo waves on the video monitor.

(a)

(b)

Figure 9.2 Flow condition at #2 (V_W, V_O) = (0.55, 0.76) ft/sec of figure 6.1.

(a) Bamboo waves in up flow on the left, and DCAF with mild corkscrew waves on the right.

(b) Bamboo waves on the video monitor.

(a)

(b)

Figure 9.3 Flow condition at #3 (V_w, V_o) = (0.55, 0.46) ft/sec of figure 6.1.

(a) Bamboo waves arising from shear stabilization of slugs in up flow on the left, corkscrew waves on the right.

(b) Bamboo waves on the video monitor.

(a)

(b)

Figure 9.4 Flow condition at #4 (V_w, V_o) = (0.55, 0.35) ft/sec of figure 6.1. The flows are like those in figure 9.3, but exaggerated.

(a)

(b)

Figure 9.5 Flow condition at #5 (V_w, V_o) = (0.27, 0.31) ft/sec of figure 6.1.

(a) Bamboo waves in up flow on the left, DCAF with corkscrew waves on the right.

(b) Bamboo waves on the video monitor.

(a)

(b)

Figure 9.6 Flow condition at #6 (V_w, V_o) = (0.27, 0.46) ft/sec of figure 6.1.

(a) Bamboo waves in up flow on the left, corkscrew waves on the right.

(b) Bamboo waves on the video monitor.

(a)

(b)

Figure 9.7 Flow condition at #7 (V_w, V_o) = (0.27, 0.61) ft/sec of figure 6.1.

(a) Bamboo waves in up flow on the left, mildly disturbed core annular flow in down flow on the right.

(b) Bamboo waves on the video monitor.

(a)

(b)

Figure 9.8 Flow condition at #8 (V_w, V_o) = (0.27, 0.76) ft/sec of figure 6.1.

(a) Bamboo waves in up flow on the left, DCAF with immature bamboo waves on the right.

(b) Bamboo waves on the video monitor.

(a)

(b)

Figure 9.9 Flow condition at #9 (V_w, V_o) = (0.27, 0.91) ft/sec of figure 6.1.

(a) Bamboo waves in up flow on the left, DCAF with immature bamboo and corkscrew waves on the right.

(b) Bamboo waves on the video monitor.

Figure 9.10 Neutral for a=1.31 and Rg=0.4. The upper branch of the two neutral curves in figure 9.3 connect on

Figure 9.11 Down flow experiment #2

Figure 9.12 Down flow experiment #3

Figure 9.13 Down flow experiment #3, perfect CAF upper branch

Summary and discussion

We reported the results of experiments on water lubricated pipelining of 6.01 cylinder oil in a vertical apparatus with up and down flow. The measurements were compared with theoretical predictions based on ideal laminar flow (PCAF) and with the linear theory of stability.

Flow rates for the oil and water, pressure gradients and holdup ratios for up and down flow over a wide range of velocities less than 3 ft/sec were recorded.

The oil is buoyed up in water by gravity. In up flow the pressure gradient and buoyancy are in the same direction. Waves develop in up flow and the lubrication forces together with the buoyancy tend to stretch wave troughs. In down flow the pressure gradient and buoyancy are opposed. This compresses the oil column, suppresses bamboo waves, and leads to straight or buckled columns of oil. The differences between up and down flow are suppressed in fast flow when the pressure gradient dominates buoyancy.

The stretching of oil in up flow and its compression in down flow implies that less oil will accumulate in down flow than in up flow. It is possible to fluidize hugely long slugs of oil in down flow.

The ratio of the input ratio to the volume ratio is called the holdup h; h is one in a well-mixed flow and larger than one in a laminar lubricated flow without gravity. Buoyancy changes this; zero and even negative holdups are possible (see figure 8.1).

Different types of flow were observed and located on flow charts in a V_W, V_O plane. The flow types change with the oil flow at a fixed water flow.

First we describe changes in up flow as the oil flow is increased. For slow oil flow with enough water, oil bubbles will form by capillary instability; if the water flow is fast enough the large bubbles are torn apart, leaving o/w dispersions. When the water flow is slow enough to support capillary bubbles, increasing oil flow will cause the bubbles to connect into longer structures, called slugs, which are like

segments of bamboo with bamboo swells connected by long thin bamboo stems. Further increases in the oil flow cause the segments to connect into a definite bamboo train. The stems of the bamboo thicken and the distance between the cells decreases with increasing oil flow. Bamboo waves seem to be imperfect monochromatic waves with a very well defined average length, speed and amplitude. Yet further increases in the oil throughput lead to much thicker and shorter stems and the bamboo crests become very jagged, irregularly not axisymmetric. These are called disturbed bamboo waves (DBW). BW and DBW are robust regimes of up flow.

In a certain region of the up flow chart, small water flow and large oil flow, the oil sticks to the wall. This is a flow induced adhesion, and it can be reversed. This flow induced "change of adhesion" results either in blockage with a loss of lubrication or in a three-layer configuration with oil on the outer wall, water in an annulus beneath and oil in the core. Our apparatus could not withstand the pressures needed to produce larger rates of oil than the ones in which oil sticks to the wall. We believe that water in oil emulsions would arise if the oil flow could be increased.

Now we describe down flow after the flow turns at the bend at the upper end of the pipe, first for high oil flows with DBW in up flow and then as the oil flow is decreased. When DBW are observed at high oil flow rates in up flow, they are also observed in down flow. However, the wave lengths of DBW are shorter in down flow than in up flow because of stretching in up flow and compression in down flow. When the oil input is decreased, the waves disappear leading to disturbed core annular flow. This flow can be almost a perfect core annular flow. At higher flow rates of oil, it is disturbed by immature bamboo waves, at lower flow rates by rotating buckled structures which we call corkscrews. At yet lower oil inputs the oil column will break into trains of longs slugs and then into trains of large bubbles which seem tied together by wake forces.

For a fixed flow of oil, there is an optimum flow rate of water for which the pressure gradient is a minimum. The minimum pressure gradient is in a region of bamboo waves in up flow and in a region of

disturbed core annular flow in down flow. The pressure gradients in down flow are less than in up flow. This shows that disturbed core annular flow is more efficient than bamboo waves.

Some new formulas for perfect core annular flow are derived and used to compare ideal lubrication theory with experiments and to obtain some measures of energy efficiency. To make the dynamic pressure gradient appear explicitly, it is necessary to take account of the overburden based on the composite water-oil density. The is no static solution of the PCAF problem, so that the treatment of hydrostatic gradients requires thought, and it leads to the decomposition of the governing equations in which the density appears only in terms of the density difference $\hat{u}\rho\hat{o}$, as expected. These equations are easily integrated and all quantities can be evaluated on this PCAF solution when two parameters, like flow input of oil and water, are prescribed. A theoretical formula for the holdup is derived and evaluated. We find the water fraction for the PCAF flow for which the oil flow is maximum when the pressure gradient is fixed.

We compared measured pressure gradients with different ideal pressure gradients in five cases of up flow and five cases of down flow. The pressure gradient required to move a given flow rate of 6.01 poise oil is on the average 200 times greater when there is no water lubrication. This improvement is roughly one-third of the ratio $\mu_o/\mu_w=1/m$. We can guess that drag reductions of the order $\mu_o/3\mu_w$ are possible in a vertical pipeline. For a viscous crude, water lubrication would reduce the pressure gradient by a factor of more than 10,000.

We compared measured pressure gradients with the gradients required to move water alone with a flow rate equal to measured total flow, oil plus water. For laminar flow, the measured gradients in lubricated flow are roughly three times larger than the theoretical gradients required for laminar flow of water alone. However, at the given flow rates water would be in turbulent flow and the ratio of measured to theoretical values much closer to one.

The measured values of the pressure gradient and water fraction were compared with theoretical values computed for PCAF with the same oil and water input. The computed water fraction expressed by

the radius ratio $a=R_2/R_1$ is smaller than the mean values $a_e=R_2/R_{1e}$ measured in the experiments. This reduction in the water fraction is due to the transport of water trapped between bamboo waves, flushing out water, leaving a smaller water fraction behind. The computed pressure gradients in up flow at low oil flow rates is much smaller than measured values. This comparison has no significance because under these conditions the motive force of transport is buoyancy. At higher oil flow rates, the ratio of computed to measured pressure gradients of is order one, between ?.

Theoretical and measured values of the water fraction and pressure gradients in down flow are very close. This shows that realized down flows called disturbed core annular flows are practically optimally efficient, with pressure gradient reductions of the same value as PCAF with the same water fraction. This is because DCAF is at most a perturbation of PCAF. The measured gradients of pressure are not globally optimal, however, because there is another PCAF, with a different and best water fraction, for which the pressure gradient for a given flux of oil is minimum.

We compared measured values of the speed and wave length of bamboo waves with two different theoretical values computed from the linear theory of stability. In the first comparison we compared all flows with the same oil and water input, the same V_o and V_w, as in our experiments. In the second comparison we compared all flows with the same oil input and water fraction, the same V_o and a, where a was put equal to the measured value for that V_o. The second comparison was introduced to validate the following conclusion: the wave on a very viscous oil, which basically must travel with nearly uniform velocity (see figure 8.1), must be very nearly a standing wave, convected with the flow. A 6.01 poise is too viscous to support fast wave propagation. In every case, computed wave speed c of the most unstable disturbance was nearly the same as the speed W of the oil core in the basic PCAF.

The average wave length of bamboo waves is slightly larger than the wave length of the most unstable disturbance of a $PCAF_1$, with the same V_o and V_w and also of the $PCAF_2$, with the same V_o and a as in the experiments. Nonlinear effects are responsible for stretching the stems of bamboo waves, explaining the small discrepancy between linear stability theory and experiments.

There is a larger discrepancy between the measured and theoretical wave speeds for PCAF, with up to three times faster speeds found in computations. We attribute this discrepancy to a systematic difference $a–a_2>0$ between experiments and $PCAF_1$. The wave speed must be greater for flows with more water because the oil core with superficial oil velocity V_o has to rise faster when a is larger. Since the wave is convected with the oil, a comparison of computation with one a with another computation or experiment with another? will give rise to a systematic discrepancy of the observed type. In fact this systematic discrepancy disappears when the measured speeds are compared with the ones computed for the $PCAF_2$ which has the same a.

We attempted to predict the flow types observed in experiments by identifying the source of instability in the terms of the energy equations which we computed for the most dangerous disturbance of $PCAF_1$ and $PCAF_2$. For $PCAF_1$ we found that in all cases in which oil bubbles and slugs in water were observed, the instability arises from the boundary through a combination of interfacial tension and interfacial friction. In the region where bamboo waves and disturbed bamboo waves were observed, only interfacial friction acts to produce instability either of $PCAF_1$ or of $PCAF_2$. For $PCAF_1$, analysis of down flows gives rise to the same satisfying identifications of the sources of instability of slug flow and disturbed bamboo waves. In addition for the two arbitrarily chosen points near the center of the DCAF, where nearly perfect core annular flows are actually observed, the linear theory shows $PCAF_1$ to be stable. PCJ and HJa showed that in all cases where oil in water dispersions were observed, instability of PCAF arises from the Reynolds stress in the water, and not from terms at the boundary. We did not observe o/w dispersion in the experiments and no term with a Reynolds stress induced instability was identified in the theory.

Future work correlating stability calculations with experiments using more viscous and less viscous oils in vertical flow ought to be undertaken. It is especially important to build a robust apparatus in which the pressure gradients needed to create o/w emulsions can be attained. The transition to o/w emulsions is a practical problem of considerable importance because it leads to a loss of lubrication in the field.

Acknowledgements

This work was supported by the Department of Energy; the Army Research Office, Mathematics; the National Science Foundation, fluid mechanics; and the Supercomputer Institute. R. Bai's work was supported in part by the People's Republic of China. We wish to thank Mike Arney for his work on the measurement of the material parameters of the fluids used in the experiments. We are indebted to Veet Kruka and Greg Geiger, at Shell development in Houston, for sharing their knowledge of the applications side of this subject, and in general, for moral and logistical support from the beginning of our studies of lubricated pipelining.